Available online at www.sciencedirect.com

ScienceDirect

Geochimica et Cosmochimica Acta 246 (2019) 461–477

Geochimica et Cosmochimica Acta

www.elsevier.com/locate/gca

Iron isotope constraints on planetesimal core formation in the early solar system

Michelle K. Jordan *, HaoLan Tang, Issaku E. Kohl, Edward D. Young

Department of Earth, Planetary, and Space Sciences, University of California, Los Angeles, USA

Received 18 May 2018; accepted in revised form 6 December 2018; Available online 13 December 2018

Abstract

We determined the Fe isotope fractionation between the metal and silicate phases of two aubrite meteorites, Norton County and Mount Egerton. We find that the metallic phase is high in $^{57}Fe/^{54}Fe$ with respect to the silicate phase, with $\Delta^{57}Fe_{metal\text{-}silicate} = 0.08‰ \pm 0.04$ for Mount Egerton and $0.09 \pm 0.02‰$ for Norton County. These data, combined with new measurements of $^{57}Fe/^{54}Fe$ of IIIAB iron meteorites, are used to constrain the origins of the high $^{57}Fe/^{54}Fe$ exhibited by all classes of iron meteorites. We find that if the parent bodies of the iron meteorites had chondritic bulk $^{57}Fe/^{54}Fe$ values, their cores must have been unusually small ($\leq$8% by mass). Relaxing the constraint that the bodies were chondritic in their bulk iron isotope ratios allows for larger core mass fractions commensurate with usual expectations. In this case, the elevated $^{57}Fe/^{54}Fe$ values of iron meteorites are due in part to evaporation of melt during the accretion stages of the parent bodies and not solely the result of metal-silicate differentiation.

1. INTRODUCTION

Direct sampling of metal cores of intact planets and planetesimals is impossible. Therefore, in order to understand the origin and chemical influences of planetesimal metal core formation, we must appeal to meteoritical analogs that represent disrupted planetesimals. Iron is prominent in both cores and silicate mantles of planetary bodies and is a useful tracer for planetary differentiation and core formation. Stable isotope ratios of Fe provide a tool for reconstructing the accretion histories and/or planetary differentiation processes attending core formation. In this study, we focus on the iron isotopic compositions of metal-rich meteorites and what they reveal about planetesimal cores.

The Fe isotope compositions of Earth, Moon, Mars (SNC meteorites), Vesta (HED meteorites), and several meteorite classes have been previously measured and the data exhibit variability among Solar System materials (Fig. 1) (Zhu et al., 2002; Kehm et al., 2003; Poitrasson et al., 2004; Weyer et al., 2005; Weyer and Ionev, 2007; Schoenberg and von Blanckenburg, 2006, Horn et al., 2006; Dauphas et al., 2009a,b; Craddock and Dauphas, 2011; Wang et al., 2012). One possible explanation for this variability is differences in the processes that produced the cores of these bodies.

Magmatic iron meteorites are thought to represent the cores of differentiated asteroid-sized bodies. The meteorite data indicates that these metallic cores have high $^{57}Fe/^{54}Fe$ with respect to chondritic composition by ~0.13‰ (Zhu et al., 2002; Kehm et al., 2003; Poitrasson et al., 2004; Weyer et al., 2005; Schoenberg and von Blanckenburg, 2006; Williams et al., 2006; Horn et al., 2006; Dauphas et al., 2009a,b; Craddock and Dauphas, 2011). This difference between chondrites and magmatic iron meteorites is potentially explained if the heavy isotopes of Fe partition into the metallic melt during planetary differentiation and core formation. While the disparity in iron isotope ratios

* Corresponding author.
E-mail address: mkjordan@ucla.edu (M.K. Jordan).

https://doi.org/10.1016/j.gca.2018.12.005
0016-7037/

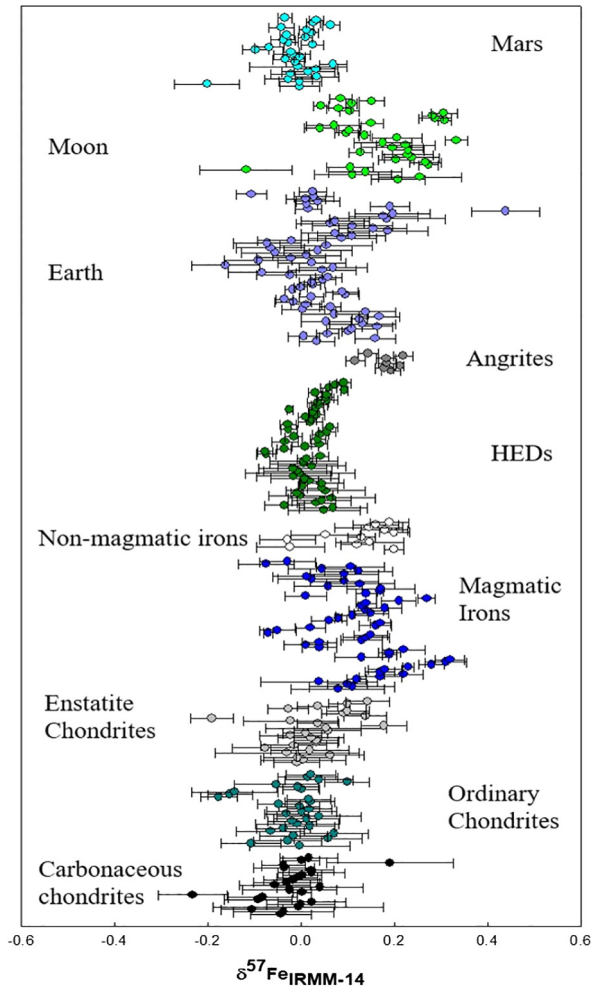

Fig. 1. The Fe isotope compositions of several planets and meteorite groups exhibiting the variability among different Solar System bodies. Note that iron meteorites, Earth, Moon, and angrites are all isotopically heavy relative to chondrite. Data are compiled from Zhu et al. (2002), Kehm et al. (2003), Poitrasson et al. (2004), Weyer et al. (2005), Weyer and Ionev (2007), Schoenberg and von Blanckenburg (2006), Horn et al. (2006), Dauphas et al. (2009a,b), Craddock and Dauphas (2011), and Wang et al. (2013).

between metals and silicates suggests that this may be the case, uncertainty arises because these rock groups are not cogenetic.

Previous experimental work and measurements of pallasite meteorites have sought to establish the equilibrium Fe isotope fractionation between metal and silicate at high temperatures, but results have been inconsistent with respect to both the sign and magnitude of Fe isotope metal-silicate fractionation (Zhu et al., 2002; Weyer et al., 2005; Poitrasson et al., 2005, 2009; Roskosz et al., 2006; Shahar et al., 2015; Elardo and Shahar, 2017; Hin et al., 2012). Pallasites contain large amounts of both silicate (olivine) and Fe-rich metal and are thought to represent the core-mantle boundaries of their asteroidal parent bodies. However, variable results have limited their usefulness. Some studies indicate that the metallic phase is high in $^{57}Fe/^{54}Fe$ relative to silicate, some show the opposite, and still others show no discernable difference in Fe isotope ratios (Fig. 2). The inconsistency may stem from variable degrees of equilibration between the olivine grains and the metallic matrix; some olivine grains may not be isotopically equilibrated with the metallic matrix (Weyer et al., 2005). Similarly, several studies have reported the Fe isotope fractionation between metal and silicate from piston-cylinder experiments at high temperatures and pressures (Poitrasson et al., 2009; Hin et al., 2012; Shahar et al., 2015; Elardo and Shahar, 2017) but with seemingly inconsistent results, although direct comparisons are complicated by differences in experimental conditions and phase compositions.

In order to determine whether or not there is an Fe isotopic signature that accompanies metal-silicate differentiation, we measured Fe isotope ratios in metal and silicate coexisting in two aubrite meteorites, Norton County and Mount Egerton. The Si isotope ratios in silicates and metals in these differentiated meteorites have already been determined to be in equilibrium (Ziegler et al., 2010), suggesting that the Fe isotopes are also in equilibrium. The solubility of Si in Fe-rich metal is temperature dependent, allowing us to estimate a temperature of equilibration for these rocks and therefore the temperature-dependent Fe isotope fractionation between silicate and metal.

We combine the derived silicate-metal Fe isotope fractionation factor with measurements of Fe isotope ratios in a suite of IIIAB iron meteorites to assess the accretion history of planetesimals and their relative core sizes as constrained by Fe isotopes. Our results suggest that evaporation of iron may have contributed to the Fe isotopic composition of the metal in planetesimals.

2. SAMPLES AND ANALYTICAL METHODS

2.1. Samples

The Norton County and Mount Egerton aubrites are differentiated igneous rocks, consisting primarily of nearly FeO-free enstatite with smaller amounts of plagioclase, diopside, olivine, metallic Fe-Ni, troilite, and other trace minerals. Unlike most aubrites, Mount Egerton is not a breccia. The FeO content of the enstatite in aubrites, in general, is much lower than that of terrestrial enstatite (Watters and Prinz, 1979). The low concentration of Fe in the silicate phase results from the extremely reducing conditions under which these meteorites formed; these rocks record some of the most reducing conditions present in Solar System materials (Casanova et al., 1993).

The metal content of aubrite meteorites is variable (0.1–2.3 vol%) with the metal possessing high concentrations of Si due to the reducing conditions under which it formed; Si becomes more siderophile at low oxygen fugacity (Casanova et al., 1993; Wade and Wood, 2005). Metal is present as small inclusions in the enstatite grains, submicron-sized blebs in the matrix, irregularly-shaped grains up to several hundred micrometers, and larger centimeter-sized nodules. The metal is predominantly kamacite and has sulfide and silicate inclusions concen-

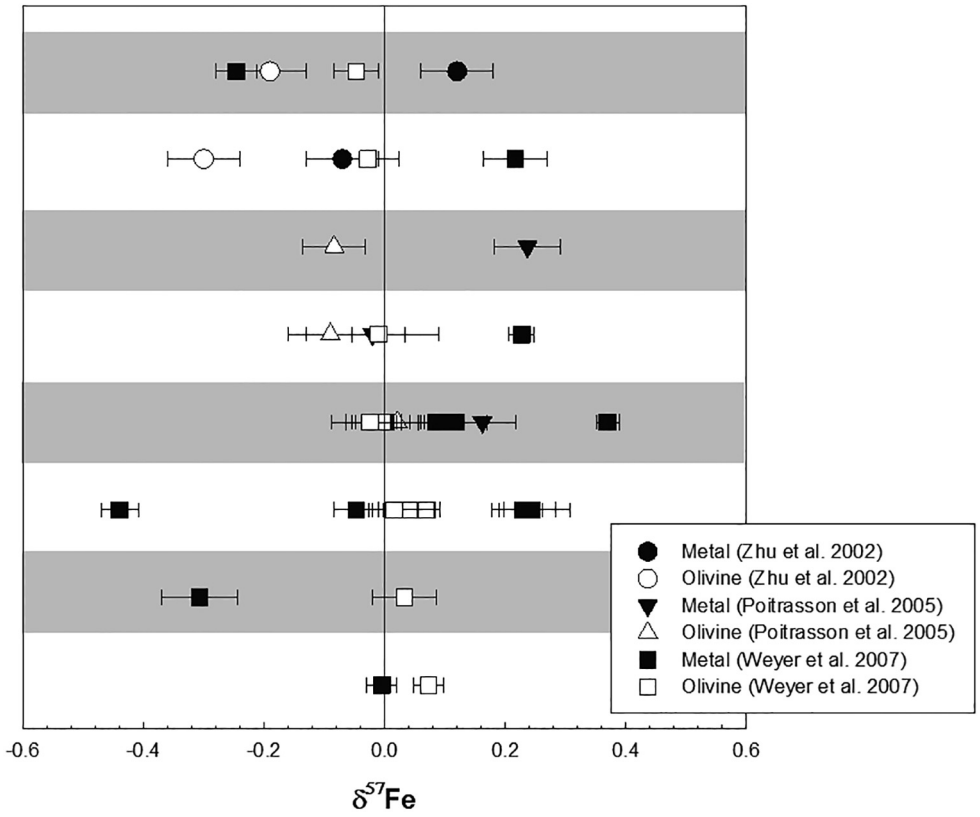

Fig. 2. Compilation of $^{57}Fe/^{54}Fe$ measurements of paired olivine and metal separates from pallasites as reported in the literature. Black symbols represent metal separates and white symbols represent olivine separates. Various shapes indicate that the data were collected from different groups. Each white or gray band corresponds to a specific pallasite meteorite. The studies attempt to measure the equilibrium Fe isotope fractionation between metal and silicate, but show no systematic trend. Data are compiled from Zhu et al. (2002), Poitrasson et al. (2005), and Weyer et al. (2007).

trated towards the grain edges, though these inclusions are rare. Both schreibersite and perryite are frequently associated with metal grains, with perryite only existing in the larger centimeter-sized nodules (Casanova et al., 1993). Casanova et al. (1993) suggest that the metal in aubrite meteorites represents residual material trapped in a silicate magma during partial melting. A depletion of Cr in aubrites relative to CI chondrites suggests that the metal itself has not undergone fractional crystallization (Casanova et al., 1993).

Ziegler et al. (2010) measured the silicon isotope ratios in the metal and silicate phases of these meteorites and determined the $^{30}Si/^{28}Si$ fractionation between the phases. The agreement in temperature-dependent fractionation between that measured in the meteorite, ab initio calculations, and an experimental determination (Shahar et al., 2009, Ziegler et al., 2010) has been taken as strong indication that the Si in metal and in silicate is in isotopic equilibrium. Given the evidence for Si isotopic equilibrium in these rocks, we infer that Fe is also in isotopic equilibrium, making the rocks suitable for our purposes. However, the temperature of equilibration is revisited in this study.

Norton County (Fig. 3A) is the largest recovered aubrite meteorite. The brecciated meteorite consists of 84.5 vol% enstatite with forsterite, diopside, and plagioclase making up most of the remaining silicate material (Watters and Prinz, 1979). The enstatite in Norton County contains about 0.07 wt.% FeO. The low concentration of Fe in the silicate material makes measurements of the Fe isotope composition of this phase challenging. The metal occurs mainly as irregularly shaped grains and accounts for about 1–1.5 vol.% of the meteorite (Watters and Prinz, 1979; Okada et al., 1988; Casanova et al., 1993). It consists largely of kamacite, with 1.4–2 vol.% perryite, and up to 6 vol.% schreibersite (Watters and Prinz, 1979). The kamacite is principally Fe with ~0.91 wt.% Si and ~ 4.7 wt.% Ni (Watters and Prinz, 1979). Our sample of Norton County comes from the University of New Mexico collection (care of Prof. Carl Agee). In total, ~104 g of Norton County were obtained; the large sample mass allows for extraction of sufficient silicate-hosted iron to yield a reliable measurement of Fe isotope ratios. We sampled large metal nodules in order to ensure that the metal phase could be easily identified and isolated.

Mount Egerton (Fig. 3B) is an unbrecciated meteorite from Western Australia (McCall, 1965). It is often classified as an anomalous aubrite due to its relatively high metal content as compared to other aubrite meteorites (Casanova et al., 1993; McCall, 1965). The silicate portion of the meteorite is composed primarily of large enstatite

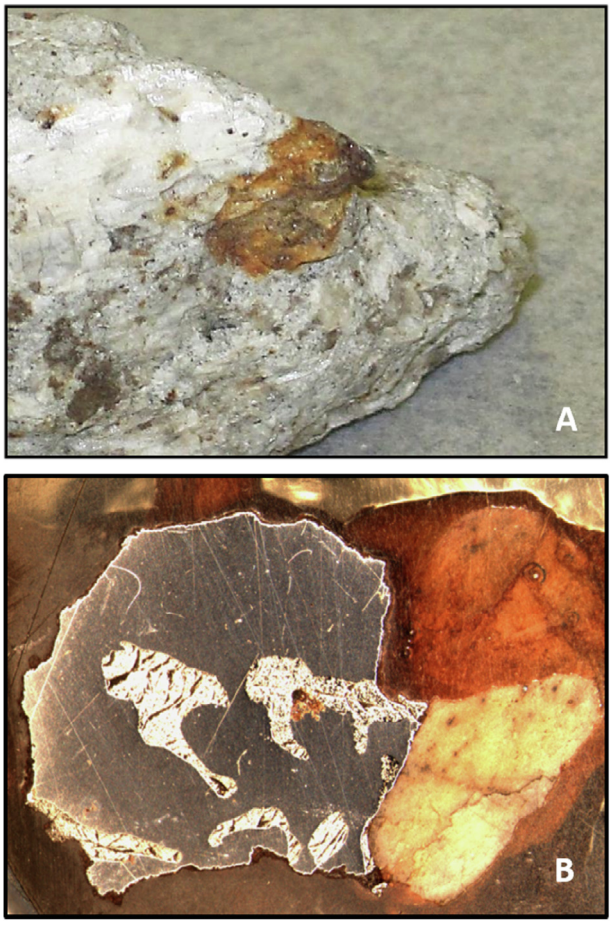

Fig. 3. (A) Photograph of the Norton County aubrite meteorite showing large enstatite crystals and metal nodules and blebs. (B) Thick section of Mount Egerton showing both the metal and silicate phases. Aubrites were formed under reducing conditions and have significant Si in the metallic phase and minimal Fe in the enstatite as a result.

crystals with smaller amounts of diopside (Watters and Prinz, 1979). Similar to Norton County, the enstatite phase contains 0.07 wt.% FeO. The metal, which appears as cm-sized blebs, is kamacite and comprises about 21 wt.% of the meteorite; perryite is associated with the metal phase (Watters and Prinz, 1979; Wait, 1970; Wasson and Wai, 1970; Casanova et al., 1993). Troilite and schreibersite are minor phases in Mount Egerton (Wasson and Wai, 1970; Watters and Prinz, 1979, 1980; Watters et al., 1980). The kamacite in Mount Egerton contains ~2 wt.% Si and ~6.25 wt.% Ni, with some metal inclusions in the enstatite containing up to 8.25 wt.% Ni (Watters and Prinz, 1979, 1980; Watters et al., 1980). The Mount Egerton samples come from the UCLA collection and consisted of a piece that was mainly silicate material, weighing about 4.5 g and a separate metal slice weighing ~340 mg.

The redox reaction involving oxidized and reduced forms of Si and Fe can be used to calculate equilibration temperatures for highly reduced meteorites because the equilibrium expressed in the redox reaction is temperature dependent (Laramir, 1968; Wasson et al., 1994). Once an equilibration temperature has been established, it can be used to calibrate the temperature dependence of Fe isotope fractionation between these phases. The reaction involves the two most abundant phases, enstatite and kamacite. Wasson et al. (1994) used the reaction $2[FeSiO_3]_{pyx} + [Si]_{Fe\text{-}Ni} = 2[Fe]_{Fe\text{-}Ni} + 3[SiO_2]_{crist}$ to estimate the temperature of Si equilibration in metal. When applied to Norton County, this method suggests an equilibration temperature of 1130 K ± 80 K. For Mount Egerton the same reaction yields a temperature of 1200 K ± 80 K. Uncertainties in the activity coefficients and Gibbs free energies of reaction limit the accuracy of these estimated equilibration temperatures (Wasson et al., 1994; Ziegler et al., 2010).

In addition to the aubrite meteorites, we also measured the Fe isotope composition of several magmatic iron meteorites in order to assess whether or not fractional crystallization could have affected their Fe isotope compositions. There are several groups of iron meteorites with varying formation and thermal histories; the groups are classified by their chemical trends. For the magmatic iron groups, or non-silicate bearing groups, the compositional trends suggest solidification of a core from a metallic melt by fractional crystallization as the parent body cooled (Scott, 1972; Scott and Wasson, 1975). The fractional crystallization has been modeled using the Rayleigh equation (Wasson, 1999). Other processes such as assimilation of additional metal, dendritic crystallization, the onset of liquid immiscibility, and incomplete mixing of the molten core may complicate the history of these iron meteorites, but fractional crystallization seems to have dominated (Goldstein et al., 2009).

Group IIIAB iron meteorites were used for Fe isotopic analysis in this study. IIIABs are the most populated iron meteorite group as well as the group with the most well-defined fractional crystallization elemental trends (Goldstein et al., 2009). Negative correlations between the concentrations of several incompatible elements, including As, and compatible elements, including Ir, define the degrees of fractional crystallization in IIIABs (Wasson, 1999). We use the relative concentrations of highly incompatible As as a measure of the degree of fractional crystallization. We measured the $\delta^{57}Fe$ of six magmatic iron meteorites from the IIIAB group with varying As contents (see Results below), and thus varying degrees of fractional crystallization, in order to determine if there is a systematic difference in $\delta^{57}Fe$ that could be correlated with the degree of fractional crystallization. The meteorites with higher concentrations of As, representing higher degrees of fractional crystallization, are Grant (15.5 μg/g As), Mount Edith (15 μg/g As), and Buenaventura (19.2 μg/g As) compared with the less evolved rocks that include Haig, Henbury, and Williamstown with As concentrations of about 3 μg/g. All iron meteorite samples are from the UCLA collection.

Our Fe isotopic measurements of iron meteorites are motivated by the study from Hopp et al. (2018) in which Ru isotope ratios were obtained for a collection of magmatic iron meteorites with varying degrees of fractional crystallization. Among the samples in that study were

Henbury and Grant, representing samples with very different degrees of fractionation and allowing for direct comparison with our study. Hopp et al. (2018) found that the IIAB and IIIAB magmatic iron meteorites displayed a correlation between degree of fractional crystallization and Ru isotope ratios. $\delta^{102/99}$Ru values range from ~0‰ for those samples with low degrees of crystallization (e.g., Henbury) to ~0.85‰ for samples representing larger fractions of crystallization (e.g., Grant). This result suggests that the lighter isotopes of Ru favor the solid metal phase, leaving the remaining melt enriched in the heavy isotopes of Ru.

Lastly, we measured the iron isotopic composition of several CM chondrite meteorites whole rocks as a reference for comparison with the differentiated bodies.

2.2. Phase separation, dissolution, and ion exchange chromatography

A single fraction of ~400 mg of silicate was analyzed for both aubrite samples. The use of a single aliquot was necessitated by the large amount of material required to obtain enough Fe for an accurate measurement. Silicate fractions of the aubrite meteorites were obtained by breaking off sizable enstatite crystals from larger pieces of both Norton County and Mount Egerton. Sample edges were abraded with silicon carbide to remove any lingering Fe-oxide. The enstatite crystals were crushed into fine grains using an agate mortar and pestle; metallic particles were removed from the powder using a hand magnet. A Frantz Magnetic Separator followed by handpicking were also employed to remove sulfide and other minor phases before dissolution. We dissolved four samples of Norton county metal and two samples of Mount Egerton metal each with masses of ~30 mg. About 0.1 mg of each sample was purified for analysis. Metal samples for the aubrites and the IIIAB iron meteorites were cut using a diamond-blade saw. In the case of Norton County, we cut metal nodules away from the silicate mass; for Mount Egerton and the iron meteorites, we cut already isolated metal pieces into smaller fragments. Iron oxides were removed by abrading with silicon carbide.

Silicate samples were dissolved on a hotplate in a 3:1 mixture of concentrated HF and HNO_3 in sealed Savillex Teflon beakers at ~155 °C. After evaporation of the HF-HNO_3 mixture, samples were sequentially fluxed and evaporated in concentrated HNO_3, concentrated HCl, and aqua regia to fully dissolve the sample. The dissolution procedure follows that described in Baker et al. (2012). Metal samples were dissolved in concentrated HCl in sealed Savillex Teflon beakers on a hotplate at ~125 °C. The solution was repeatedly centrifuged and decanted to remove any undissolved silicate material that was otherwise unable to be removed from the metal sample. Aliquots from the metal solution were fluxed in concentrated nitric acid to ensure that all Fe was present in the same oxidation state before being loaded onto resin columns.

Both metal and silicate samples were loaded onto an anion exchange column to isolate pure Fe. The silicate Mg:Fe ratio of ~500:1 required adjustment of typical separation procedures to prevent column overload.

Column Procedure for Silicate Samples. Iron from the aubrite silicate samples as well as the chondrite samples was purified following the method described by Dauphas et al. (2009a,b). Columns contained 1 mL of pre-cleaned AG1-X8 anion exchange resin (200–400 mesh). Once loaded into the column, the resin was then cleaned again with the following routine: 10 mL 18 MΩ H_2O, 10 mL 1 N HNO_3, 10 mL 18 MΩ H_2O, and 10 mL 0.4 N HCl to remove and Fe that may have been present. The column was then conditioned with 5 mL of 6 N HCl. The sample was loaded in ~0.5–1 mL 6 N HCl, depending on sample size. Non-Fe elements were eluted with 8 mL of 6 N HCl. Fe was eluted using 8 mL of 0.4 N HCl and collected in a clean Savillex beaker. The entire procedure is repeated a second time to ensure purity of the Fe. After collection, samples are dried down to a solid on a hot plate and dissolved again in 1 mL of 2% HNO_3 for analysis.

Column Procedure for Metal Samples. Smaller columns, in terms of both length and volume of resin, were used to purify Fe from the metal samples. Bio-rad Poly-Prep columns filled with AG 1 – X8 resin (100–200 mesh, chloride form) were used. The volume of resin was adjusted to 0.3 mL. The resin was cleaned with 10 mL of 9 N HCl, 10 mL of 18 MΩ H_2O, 10 mL of 9 N HCl, and 10 mL of 18 MΩ H_2O. The column was then conditioned with 6 mL of 0.5 N HCl and 3 mL of 9 N HCl. Samples were loaded in 300 μL of 9 N HCl. The beaker was washed with 500 μL of 9 N HCl. Matrix elements were eluted using 5 mL of 9 N HCl while Fe was eluted with 4 mL of 0.5 N HCl and collected in clean Savillex Teflon beakers. Samples were dried down on a hot plate at 125 °C and subsequently dissolved in 1 mL of 2% HNO_3 for analysis. Procedural blank was 2 ng Fe for this study and is a factor of 1400× smaller than the Fe comprising the least massive sample analyzed.

2.3. Mass spectrometry

Isotope ratio data were collected on a ThermoFinnigan Neptune™ multiple-collector inductively coupled plasma-source mass spectrometer (MC-ICP-MS). Samples were run in wet plasma mode. $^{54}Fe^+$, $^{56}Fe^+$, $^{57}Fe^+$, and $^{58}Fe^+$ ion beams were measured simultaneously in Faraday cups with 10^{11} Ω amplifier resistors with ion currents between $\sim 6 \times 10^{-11}$ and 1.0×10^{-10} A for ^{56}Fe. Samples were run at a mass resolving power (instrumental m/Δm) of >8500 to eliminate interferences from $^{40}Ar^{14}N^+$ and $^{40}Ar^{16}O^+$; tests demonstrated isotope fidelity with this mass resolving power. Corrections for instrumental mass bias were made using sample-standard bracketing and peak height matching between sample and standard to within 5% of the standard's signal strength for each measurement block. Samples and standards were measured in alternating blocks of 20 cycles with integration times of ~4 s per cycle and 200-s wash times to eliminate the possibility of cross-contamination between the sample and standard. We used a 2 σ rejection protocol. Samples were measured against our in-house SPEX CertiPrep® 2 standard except where otherwise noted. We report our values relative to the Fe

Table 1
Fe isotope meteorite data collected for this study. Values for δ^{57}Fe (‰) are reported relative to the Fe isotope standard IRMM-14.

Sample	Type	Avg. [Ni] (wt.%)[a]	$\delta^{56}Fe_{IRMM-14}$	2 s.e.	$\delta^{57}Fe_{IRMM-14}$	2 s.e.	Blocks
Norton County Metal 1	Aubrite		0.030	0.031	0.044	0.033	5
Norton County Metal 2	Aubrite		0.014	0.036	−0.022	0.041	6
Norton County Metal 3	Aubrite		0.039	0.014	0.050	0.026	16
Norton County Metal 4	Aubrite		0.016	0.012	0.049	0.025	21
Norton County Metal (Avg.)	**Aubrite**	**4.7**	**0.025**	**0.012**	**0.030**	**0.035**	
Norton County Silicate	Aubrite		−0.036	0.015	−0.058	0.019	15
Mount Egerton Metal 1	Aubrite		0.011	0.012	0.032	0.018	14
Mount Egerton Metal 2	Aubrite		−0.006	0.011	0.016	0.017	15
Mount Egerton Metal (Avg.)	**Aubrite**	**6.0**	**0.002**	**0.017**	**0.024**	**0.015**	
Mount Egerton Silicate	Aubrite		−0.038	0.007	−0.052	0.012	42
Haig	IIIAB iron	7.32	0.041	0.010	0.061	0.016	29
Williamstown	IIIAB iron	7.38	0.098	0.009	0.142	0.016	23
Henbury	IIIAB iron	7.59	0.098	0.016	0.141	0.021	23
Grant	IIIAB iron	9.29	0.062	0.007	0.101	0.014	23
Mount Edith	IIIAB iron	9.37	0.106	0.011	0.168	0.018	23
Buenaventura	IIIAB iron	9.77	0.125	0.010	0.169	0.016	26
Murchison	CM chondrite		−0.003	0.015	−0.010	0.041	20
Murchison	CM chondrite		0.000	0.014	0.003	0.028	20
Murray	CM chondrite		0.008	0.012	0.020	0.018	20
Murray	CM chondrite		−0.025	0.018	−0.030	0.031	20
Nogoya	CM chondrite		−0.017	0.017	−0.020	0.037	20
Nogoya	CM chondrite		−0.004	0.013	0.012	0.022	20

[a] Ni concentrations for aubrites are from Watters and Prinz (1979, 1980) and Watters et al. (1980). Ni concentrations for the IIIAB meteorites are from J. Wasson Unpub.

standard IRMM-14 based on measurements of our SPEX CertiPrep® 2 standard against IRMM-14. During the duration of this study the SPEX CertiPrep® 2 was measured 20 times (20 blocks of 20 cycles) relative to IRMM-14 to yield $\delta^{56}Fe = 0.525‰ \pm 0.017$ (2 s.e.) and $\delta^{57}Fe = 0.774‰ \pm 0.021$ (2 s.e.). Each reported sample measurement is the average of between 5 and 21 blocks for metals and 15–42 blocks for silicates as dictated by the masses of Fe for each of the samples.

We tested the column chemistry procedures for isotope fidelity using elemental SPEX CertiPrep® solutions mixed with a matrix composition approximating that of the silicate portion of Norton County. Aliquots of the mixture were processed on the columns according to our procedures and then compared with unprocessed, pure Fe SPEX CertiPrep®. No differences in Fe isotopic composition were resolved. We also analyzed the eluted matrix to confirm the absence of Fe. Similar tests were performed for solutions mimicking the Fe-Ni alloy and using the relevant column procedure. In addition, we measured the Fe isotope ratios for the USGS basalt standard BCR-2 three times using our chemistry procedures and obtained δ^{56}Fe and δ^{57}Fe values of 0.090‰ ± 0.010 (2 s.e.) and 0.126‰ ± 0.023 (2 s.e.) as measured directly relative to IRMM-14 which compare favorably with the values of 0.091 ± 0.011 (95%) and 0.126 ± 0.017 reported by Craddock and Dauphas (2011). These can be compared with three analyses of IRMM-14 itself yielding δ^{56}Fe and δ^{57}Fe values of 0.002 ± 0.005 (2 s.e.) and 0.004 ± 0.007 (2 s.e.) relative to IRMM-14.

3. RESULTS

Fe isotope compositions for each meteorite and/or phase are reported as per mil deviations from the standard IRMM-14, δ^{57}Fe (Table 1). The average δ^{57}Fe values for the metal fractions from Norton County and Mount Egerton are 0.030‰ ± 0.035 (2 s.e.) and 0.024‰ ± 0.015 (2 s.e.), respectively. The average δ^{57}Fe values for the silicate fractions are −0.058‰ ± 0.019 (2 s.e.) and −0.052‰ ± 0.012 (2 s.e.), respectively. The calculated metal-silicate isotopic fractionation, $\Delta^{57}Fe_{metal\text{-}silicate}$, is 0.08‰ ± 0.04 (2 s.e.) for Norton County and 0.09‰ ± 0.02 (2 s.e.) for Mount Egerton (Fig. 4). The positive value indicates that the heavy isotopes of Fe preferentially partition into the metallic phase during metal-silicate differentiation.

The measured CM chondrite whole rock samples from our study span a range of δ^{57}Fe values from −0.030 to 0.020‰. These data fall within the typical range of Fe isotope compositions for carbonaceous chondrites. The average value is −0.004‰ ± 0.008 (2 s.e.).

The δ^{57}Fe values for the IIIAB iron meteorites range from +0.061 to +0.169‰ (±0.02 2 s.e.). The measured values fall within the range of values seen in the literature for both magmatic iron meteorites overall and for IIIAB iron meteorites specifically (Zhu et al., 2002; Kehm et al., 2003; Poitrasson et al., 2004; Weyer et al., 2005; Schoenberg and von Blanckenburg, 2006; Williams et al., 2006; Horn et al., 2006; Dauphas et al., 2009a,b; Craddock and Dauphas, 2011). All values for the iron meteorites are positive relative to published chondrite

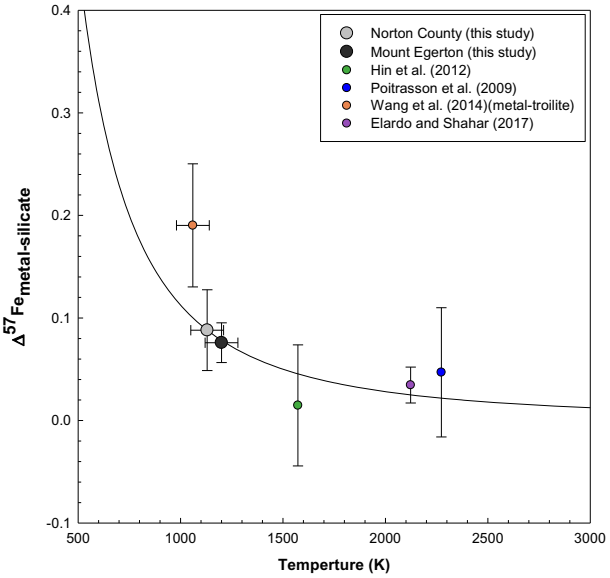

Fig. 4. Aubrite $\Delta^{57}Fe_{metal\text{-}silicate}$ and accompanying A/T^2 curve based on the measurements in this study and the temperature estimates of Wasson et al. (1994). Experimental data representing Fe isotope metal-silicate equilibrium fractionation from several other studies are plotted for reference, though direct comparison are not possible due to the varying parameters of the experiments. The metal-troilite fractionation measured by Wang et al. (2014) in natural samples is also plotted as metal-troilite fractionation is expected to be similar to metal-silicate fractionation (Polyakov et al., 2007). The point from Elardo and Shahar (2017) represents the data point with the metal composition that most closely matches the metal composition of the aubrite samples (see text). Within error, our results are broadly consistent with the experimental data.

values and those obtained as part of this study. Fig. 5 shows the iron meteorite data from this study along with carbonaceous chondrite data measured on the same instrument at UCLA, illustrating that Fe comprising the iron meteorites is indeed isotopically heavy as compared to chondrites by an amount comparable to that in the literature.

4. DISCUSSION

4.1. Fractional crystallization of cores

Firstly, we address the possibility that fractional crystallization of iron cores caused the high $\delta^{57}Fe$ values of the iron meteorites. The $\delta^{57}Fe$ values of the IIIAB samples analyzed in this study are plotted against the degree of fractional crystallization for those meteorites in Fig. 6. We use arsenic as an indicator of the degree of fractional crystallization. Arsenic is the most incompatible of the commonly reported elements, with a solid/liquid partition coefficient of $D_{As} = 0.22$ (Chabot and Jones, 2003), and thus, displays a large range of concentrations among magmatic iron meteorites. The concentration of As in the IIIAB samples relative to the concentration in the least evolved sample provides a measure of the fraction of melt remaining, F, according to the relation

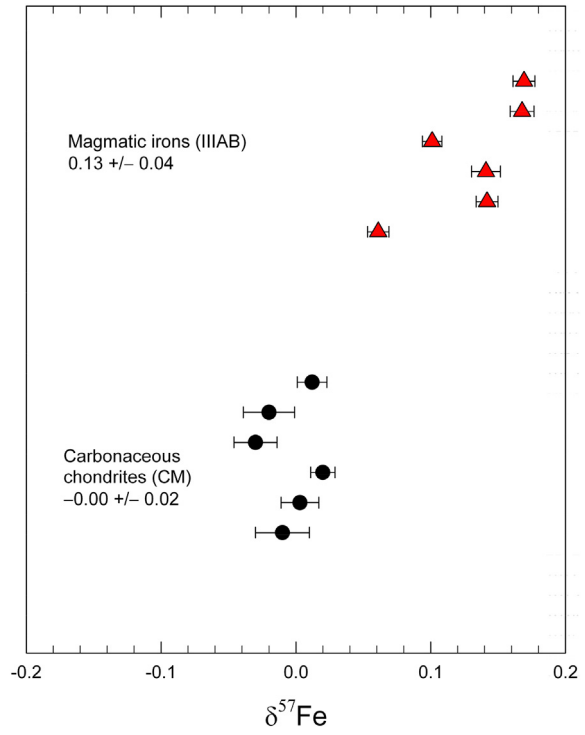

Fig. 5. Fe isotope compositions for IIIAB iron meteorites and CM chondrites measured at UCLA. The difference in composition measured in our lab is the same as that from the literature data; magmatic iron meteorites are enriched in $^{57}Fe/^{54}Fe$ relative to chondrite by about 0.13‰.

$$\frac{C_0^{As}}{C_i^{As}} = \frac{m_0^{As}}{m_i^{As}} \frac{M_i}{M_0} \sim F_i. \quad (1)$$

Here, C_i^{As} is the concentration of As in a rock specimen i, C_0^{As} is the concentration of As in the initial metallic melt represented by the least evolved of the samples, m_i^{As} is the mass of As in the evolved liquid represented by sample i, m_0^{As} is the initial mass of As in the sample representing the parent melt, M_i is the total mass represented by specimen i, and M_0 is the total mass of the initial system as represented by the least evolved specimen. Based on the incompatibility of As, we assume, to a reasonable approximation, that $m_i^{As} \sim m_o^{As}$ (As is retained nearly perfectly in melt) and consequently, from Eq. (1) we have $C_o^{As}/C_i^{As} \sim M_i/M_o = F_i$. We take the concentration of As in the initial system to be the concentration of As in the magmatic iron meteorite sample with the lowest concentration of As (i.e., lowest concentration of incompatible elements) since the concentration of As in the melt increases as crystallization progresses. We use the As concentration as a measure of the melt remaining in a Rayleigh fractional crystallization model, and therefore the fraction of total Fe remaining in melt as fractional crystallization proceeded ($F = M_i/M_o \sim Fe/Fe_o$). For Rayleigh fractionation, $R = R_o F^{\alpha-1}$, where R is the $^{57}Fe/^{54}Fe$ ratio of the melt, R_o is the $^{57}Fe/^{54}Fe$ of the initial melt, $F = {}^{54}Fe/{}^{54}Fe_o$, and α is the solid/liquid $^{57}Fe/^{54}Fe$ isotopic fractionation factor for $^{57}Fe/^{54}Fe$.

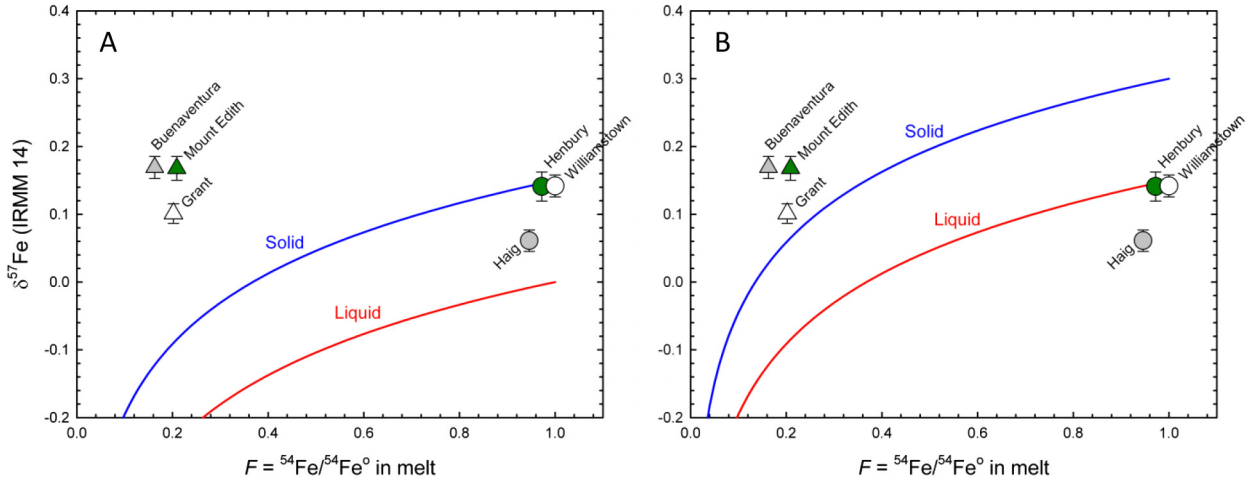

Fig. 6. The IIIAB iron meteorite data measured in this study are plotted as a function of the degree of fractional crystallization derived from the concentrations of highly incompatible elements (As in this case). A value of $F = 1$ indicates Fe resides entirely in the parental melt, while $F = 0$ indicates that all iron has crystallized as solid. There is no correlation between Fe isotope fractionation and degree of fractional crystallization. Also shown are Rayleigh fractionation curves for iron isotopes based on a $^{57}Fe/^{54}Fe$ solid/liquid fractionation factor α of 1.00015 (see text). (A) The least evolved samples are identified with the initial solids crystallized from the melt; (B) the least evolved samples are identified with the parental liquid.

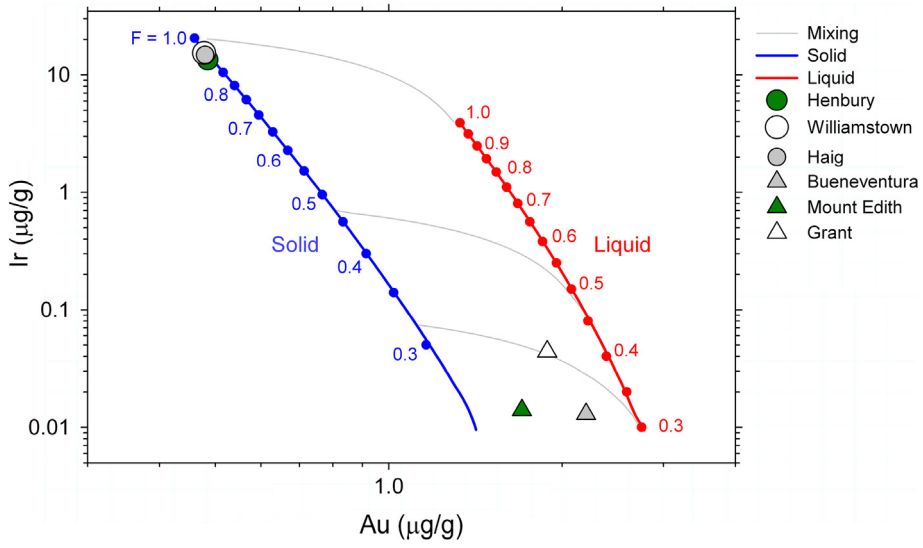

Fig. 7. Log-log plot of compatible Ir versus incompatible Au for the IIIAB iron meteorite data measured in this study (data from Wasson, 1999) and the fractional crystallization model for the IIIABs of Wasson (1999). The blue line at left shows the compositions of the solids in equilibrium with the liquids shown as the red line at right. Values for fraction of liquid remaining, F, are shown on both curves. Examples of mixing between solid and liquid are shown as the grey curves spanning the region between the solid and liquid curves. In this plot the samples shown as circles are identified as being the first solids from the parental iron metal melt, and the samples shown in triangles are crystallized from more evolved melts and include solid and trapped melt. (For interpretation of the references to colour in this figure legend, the reader is referred to the web version of this article.)

The identity of each of the IIIAB samples as either melt, solid, or a mixture of the two has been addressed previously using models for the variations in compatible and incompatible trace element concentrations. Wasson (1999) used log-log plots of Ir (compatible) vs. Au (incompatible) concentrations to show that different IIIAB iron meteorites represent solids or liquids with different degrees of fractional crystallization from a common reservoir, and that many are mixtures of solids and trapped liquid. Of the IIIAB samples analyzed in this study, Haig, Henbury, and Williamstown appear to be the first solids crystallized from pristine melts based on their relatively high concentrations of Ir and low concentrations of Au (and As) (Fig. 7). Buenaventura, Grant, and Mount Edith, on the other hand,

represent highly evolved products of fractional crystallization and are evidently mixtures of both solid and liquid (Fig. 7).

The magnitude and even the sign of the $^{57}Fe/^{54}Fe$ fractionation factor between iron-rich metal solid and liquid is not known at this writing. However, we can investigate the possibility that the uniformly high $^{57}Fe/^{54}Fe$ of the IIIAB samples might be explained by the iron-metal solid/liquid α alone with the aid of the relationships in Figs. 6 and 7. In particular, we evaluate the hypothesis that the high $^{57}Fe/^{54}Fe$ values of the IIIABs are due to crystallization of solid iron-rich metals from their parental melts. In this scenario, the IIIAB $\delta^{57}Fe$ values near 0.15‰ might suggest that $\alpha = (^{57}Fe/^{54}Fe)_{solid}/(^{57}Fe/^{54}Fe)_{liquid} = 1.00015$ if the iron melt were chondritic (we relax this constraint below). If the initial liquid was chondritic in its bulk $^{57}Fe/^{54}Fe$ ($\delta^{57}Fe = 0.0$‰), the first solids represented by Haig, Henbury and Williamstown, as suggested by their trace element concentrations (Fig. 7), would have $\delta^{57}Fe = 0.15$‰, matching the measured values (Fig. 6A). However, with continued fractional crystallization of the isotopically heavy solids, both solids and liquids evolve towards lower $^{57}Fe/^{54}Fe$ values and so the more evolved samples Buenaventura, Grant and Mount Edith samples should exhibit $\delta^{57}Fe$ values <0.0‰ rather than their values between ~0.1 and 0.2‰ (Fig. 6A). The trace element data as portrayed in Fig. 7 are not consistent with the relatively homogeneous $\delta^{57}Fe$ values of between 0.1 and 0.2‰ in this scenario.

One might hypothesize instead that that the $\delta^{57}Fe$ values of the IIIAB samples are similar to one another because of chance, perhaps due to incomplete separation of liquids and solids. Fig. 6B shows the fractional crystallization curves for the case where the least evolved rocks Haig, Henbury, and Williamstown, represent liquids rather than solids with $\delta^{57}Fe$ values greater than chondritic. Given the uncertainties in F values of about 0.1 caused by imperfect separation of solid and liquid (compare Figs. 6 and 7 where F is based on concentrations of As and on mixing models for both Ir and Au, respectively), this model could be adopted as an explanation for uniform iron isotope ratios among the IIIABs analyzed. In this scenario, and the more evolved samples Buenaventura, Grant and Mount Edith happen to have $\delta^{57}Fe$ values similar to the parental melt because they are solids crystallized from evolved melts. Coincidence between the Buenaventura, Grant, and Mount Edith data and the solid evolution curve in Fig. 6B is improved if it is recognized that trapped melt may have shifted the apparent F values of the evolved samples from ~0.3 to values near 0.1 (Fig. 7). However, this interpretation is at odds with the trace element data that suggest that the least evolved rocks are samples of the first solids to crystallize and not samples of the parental liquids (Fig. 7). Altering the sign and magnitude of the solid/liquid iron isotope fractionation factor α only exacerbates the inconsistencies highlighted here. Similarly, allowing for a subchondritic $\delta^{57}Fe$ of the core parental melt does not give rise to a solution matching the data in Fig. 6.

Evidently the limited range in IIIAB $\delta^{57}Fe$ values that are all greater than chondritic values is inconsistent with fractional crystallization of the metallic cores as the origin of these high iron meteorite $\delta^{57}Fe$ values. This conclusion is predicated on prior findings that the negative correlation between highly compatible and incompatible trace element concentrations among the IIIAB samples are the result of fractional crystallization.

4.2. Metal-silicate Fe isotope fractionation

If fractional crystallization of the core is not the explanation for high $\delta^{57}Fe$ values among iron meteorites, it may be partitioning of heavy isotopes of Fe into the metallic phase during metal-silicate differentiation, as suggested by the differences in Fe isotope ratios between metal and silicate in aubrites in this study.

We can use the equilibration temperatures for these rocks in conjunction with the measured $\Delta^{57}Fe_{metal\text{-}silicate}$ to establish a temperature calibration since isotope fractionation at high temperatures varies reliably as $1/T^2$ (Fig. 4). Using the temperatures of equilibration of 1130 K for Norton County and 1200 K for Mount Egerton, and the measured fractionation, the calibration constant A can be determined using $\Delta^{57}Fe_{metal\text{-}silicate} = A/T^2$. From A we can extrapolate over a range of relatively high temperatures for the curve. The Norton County data yield $\Delta^{57}Fe_{metal\text{-}silicate} = 1.12 \times 10^5/T^2$ and the Mount Egerton data yield $\Delta^{57}Fe_{metal\text{-}silicate} = 1.09 \times 10^5/T^2$. Experimental results are plotted for comparison in Fig. 4 as well as the fractionation between metal and troilite measured by Wang et al. (2014). Metal-silicate and metal-troilite fractionation should be similar, making this comparison relevant (Polyakov et al., 2007).

Fig. 4 shows that the data from both rocks measured in this study are consistent with some previous experimental studies (within error). However, there are some discrepancies, particularly with the experimental work of Elardo and Shahar (2017). Here we address possible explanations for the offset between the measurements in natural samples from this study and some of the prior experimental results.

One reason for discrepancies between our results and some of the earlier experimental results is differences in the compositions of the metallic phases involved. Significant concentrations of Ni and S in the iron-rich metal can increase the Fe isotope fractionation between metal and silicate (Elardo and Shahar, 2017). The greater the non-iron substitutional constituent, the larger the effect on Fe isotope fractionation. We examine this effect for the aubrite meteorites measured in this study. Elardo and Shahar (2017) found a relationship between metal-silicate fractionation factor and Ni + S concentration: $\Delta^{57}Fe_{metal\text{-}silicate} = 0.0112 \cdot (\text{at.\% Ni} + \text{S}) + 0.0346$ at 2123 K. The average compositions of our aubrite metals (Watters and Prinz, 1979, 1980) of 4.7 wt.% Ni for the metal in Norton County and 6 wt.% Ni for the metal in Mount Egerton suggest that the $^{57}Fe/^{54}Fe$ metal-silicate fractionation is ~0.085 to 0.1‰ greater than it would otherwise be if no Ni were present (at 2123 K). Adjusting for Ni concentration allows for direct comparisons between the temperature-dependent $^{57}Fe/^{54}Fe$ metal-silicate fractionation from the experimental data and our measured aubrite data. Nonetheless, even accounting for diluent Ni concentrations, the experimental data and those from the two aubrites

reported here are in disagreement, with the experimental data suggesting a greater metal-silicate fractionation.

Another factor that may be responsible for the discrepancy is the validity of the temperature of equilibration in the meteorite samples. Partial melting experiments of enstatite chondrite material can help us assess the equilibration temperature. Aubrites are likely related to enstatite chondrites as the two meteorite groups are both composed primarily of nearly Fe-free enstatite, were formed under reducing conditions, and share similar oxygen isotopic compositions (Watters and Prinz, 1979; Clayton et al., 1984; Clayton and Mayeda, 1996; Keil, 2010). Due to the similar mineralogies and apparent oxygen fugacities, enstatite chondrite partial melting experiments are relevant to the temperature of equilibration for the aubrite meteorites measured in this study. McCoy et al. (1999) conducted partial melting experiments of the Indarch enstatite chondrite and found a silicate solidus temperature of 1273 K, with the silicate being completely molten at 1773 K. Based on the Cr-Cr_2O_3 and V-V_2O_3 calibrations of Righter and Drake (200)6, the experiments were conducted at oxygen fugacities relative to the iron-wüstite buffer of approximately ΔIW= −6 to ΔIW = −8. The experiments suggest that the previously derived equilibration temperatures of 1130 K for Norton County and 1200 K for Mt. Egerton may be too low if isotopic equilibration occurred at super-solidus conditions.

A study by Berthet et al. (2009) further supports higher temperatures of equilibration for these enstatite-clan meteorites. Berthet et al. (2009) conducted partial melting experiments on Indarch. The experiments were made over a similar temperature range, but at higher pressure (1 GPa) than the ambient pressures used by McCoy et al. (1999). Additionally, the Berthet et al. (2009) experiments explored various f_{O2} conditions. The more reducing, lower f_{O_2} conditions were replicated by adding Si to the starting material at varying weight percent levels to achieve f_{O_2} values of IW – 1.5 to IW – 5. Berthet et al. (2009) found that solidus and liquidus temperatures for the silicate material increased with decreasing f_{O_2}. When melting pure Indarch with no Si metal added (∼IW – 1.5), silicate partial melting reached ∼7% at 1473 K and was completely molten at 1873 K. The solidus temperature was determined to be slightly below 1473 K. More reducing conditions further increased these temperatures. In the case where 6 wt.% Si metal was added to the starting material (IW – 4.5), the solidus temperature was above 1573 K, with silicate melting reaching 16 vol.% at 1673 K. Previous work suggests that the oxygen fugacity for aubrite equilibration is approximately 4.5–6.5 log units below the IW buffer (Righter and Drake, 2006; Casanova et al., 1993). The higher temperatures for initial melting in the Berthet et al. study compared with those from the McCoy et al. study can be explained, in part, by the higher pressures for the former; Clapeyron slopes for dry melting suggest that 1 GPa could account for melting temperatures between ∼100 and 200 K higher than those temperatures at 1 bar (10^5 Pa). The sizes of the parent bodies for these rocks are unknown, and so is the pressure of melting, but regardless, the McCoy et al. (1999) experiments and Berthet et al. (2009) experiments bracket likely melting conditions and are consistent in suggesting that the previously calculated equilibration temperatures for Norton County and Mount Egerton are too low to accommodate melting. We employ updated activity models in order to better constrain temperatures of equilibration for the aubrite meteorites analyzed in this study.

Corgne et al. (2008) investigated the effects of temperature, pressure, and melt composition on the silicate-metal partitioning behavior of several elements, including Si. Silicon behaves as a siderophile element at low oxygen fugacity. Higher temperatures also increase the affinity of Si for the metal phase, while the composition of the silicate melt and pressure have negligible effects on solubility. We apply the results from Corgne et al. (2008) to our system with the expression relating oxygen fugacity (relative to the iron-wustite buffer) to metal and silicate compositions:

$$\log\left(\frac{x_{Si}^{metal}}{x_{SiO_2}^{silicate}}\right) = a + \frac{b}{T} + \frac{cP}{T} + d\frac{nbo}{t} - \Delta IW + 2\log\left(\frac{\gamma_{FeO}^{silicate}}{\gamma_{Fe}^{metal}}\right) - log\left(\frac{\gamma_{Si}^{metal}}{\left(\gamma_{Fe}^{metal}\right)^2}\right), \quad (2)$$

In Eq. (2), a, b, c, and d are regression constants, T is the temperature in K, P is the pressure in GPa, and nbo/t is the molar ratio of non-bridging oxygens to tetrahedral cations in the silicate melt. The mole fraction of the relevant element in the relevant phase is x_M^{phase}. We use this equation to determine the equilibration temperatures based on our understanding of the activity coefficients (γ_M^{phase}) and the oxygen fugacities (f_{O_2}) under which aubrite meteorites formed. As suggested by Corgne et al. (2008), we use a value of 0.8 for γ_{Fe}^{metal} (they also suggest a value of $\gamma_{Fe}^{metal} = 1$ for the primitive mantle, we obtain the same result whether we use 0.8 or 1). The $\gamma_{FeO}^{silicate}$ is less well constrained. Corgne et al. (2008) suggest $\gamma_{FeO}^{silicate} = 3 \pm 1$ for a MgO content of ∼30 wt.%. Holzheid et al. (1997) found that silicate melts with high MgO contents increase the activity coefficient for FeO in the silicate melt. Since both Norton County and Mount Egerton have high MgO contents in the silicate material (∼40 wt.%), we evaluated the effect of MgO on $\gamma_{FeO}^{silicate}$. The experimental data from Holzheid et al. (1997) are plotted in Fig. 8. We use the resulting trend line to calculate $\gamma_{FeO}^{silicate}$ (MgO = 40 wt.%) and the associated errors. From this relationship we find that $\gamma_{FeO}^{silicate} = 5.83 \pm 0.95$ (1 S.E.). Other parameters and reference values are taken from the Corgne et al. (2008) paper and adjusted for temperature and pressure where necessary. We use an f_{O_2} of IW – 6.5 as suggested by literature values reported for aubrite meteorites (Righter and Drake, 2006). With these parameters, we find the equilibration temperatures that reproduce the Si concentrations in the metals for Norton County (0.91 wt% Si) and Mount Egerton (2 wt.% Si), yielding temperatures of ∼1415 K for Norton County and 1460 K for Mount Egerton. These temperatures are higher than the previous estimates by ∼200 degrees and are consistent with the partial melting experiments. The temperature calibrations for $\Delta^{57}Fe_{metal\text{-}silicate}$ implied by these new equi-

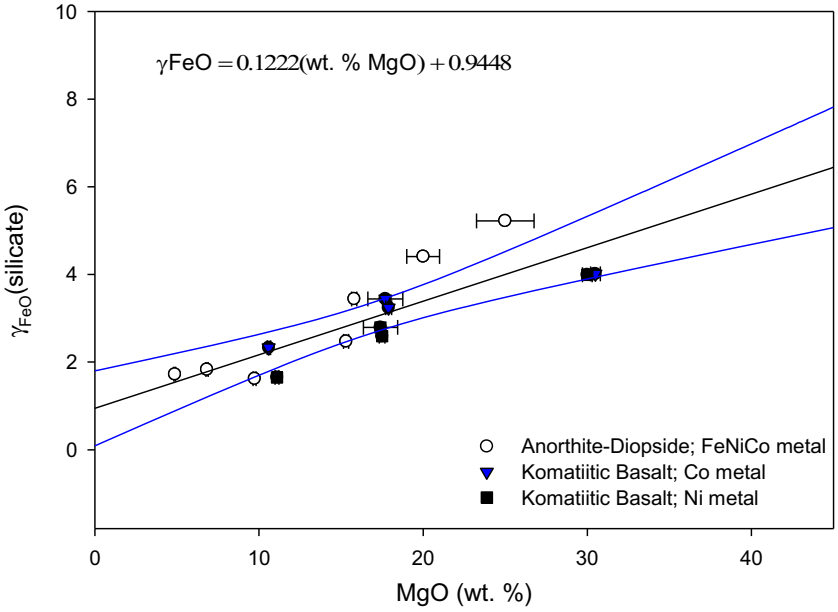

Fig. 8. Activity coefficients for FeO in silicate as a function of the MgO content of the silicate from the experiments by Holzheid et al. (1997). This trend is used to estimate the FeO activity coefficient for the aubrite meteorite silicates that have ~40 wt.% MgO. This activity coefficient is then used in the equilibrium temperature calculations.

libration temperatures and our measured Fe isotope ratio data are $\Delta^{57}Fe_{metal\text{-}silicate} = 1.6 \times 10^5/T^2$ for Norton County and $\Delta^{57}Fe_{metal\text{-}silicate} = 1.9 \times 10^5/T^2$ for Mount Egerton. The revised calibrations are plotted in the top panel of Fig. 10. The results for both a 5 and 6 wt.% Ni calibration from the experiments of Elardo and Shahar (2017) are also shown for comparison.

Error envelopes for the temperature-dependence of $\Delta^{57}Fe_{metal\text{-}siliacate}$ are based on the uncertainty of A (σ_A) in $\Delta^{57}Fe_{metal\text{-}siliacate} = A/T^2$. The uncertainty in the temperature coefficient A is

$$\sigma_A = \sqrt{T^4\sigma^2_{\Delta 57Fe} + (2\Delta^{57}Fe)^2\sigma^2_T}, \quad (3)$$

where $\sigma^2_{\Delta 57Fe}$ is the 1 s.e. uncertainty in the measured difference in isotope ratios and σ^2_T is the uncertainty in temperature. For Norton County and Mount Egerton, the temperature uncertainties are ±17.5 K arising from the uncertainties in $\gamma^{silicate}_{FeO}$ of ~±1 derived from the fit in Fig. 8, translating to uncertainties in A of $\pm 4 \times 10^4$ for Norton County and $\pm 2 \times 10^4$ for Mount Egerton (or 1–2%). For these higher temperatures assigned to the aubrites, there is marginal agreement between the experiments and the aubrite data at the extremes of the error envelopes.

The uncertainties in the activity coefficient of FeO in the silicate melt likely goes beyond those obtained from the fit in Fig. 8. Wood and Wade (2013) attempted to constrain the activity coefficient of FeO in silicate melts over a range in compositions. They amassed data for 83 experiments from several different studies in the literature, including Holzheid et al. (1997). In all of these experiments, the authors had measured the FeO content of the silicate melt in equilibrium with metal (Fe-bearing alloy) at known f_{O_2}. Wood and Wade (2013) fit the data to obtain relationship between silicate melt composition and $\gamma^{silicate}_{FeO}$. The results of this model do not agree with the relationship shown in Fig. 7. The Wood and Wade (2013) results suggest that a value for $\gamma^{silicate}_{FeO}$ of 5.83 may be too high and that the coefficient is not as sensitive to melt composition as suggested in the work of Holzheid et al. Wade and Wood provide an equation for $\gamma^{silicate}_{FeO}$ as a function of melt compositions, but the equation cannot be used to extrapolate beyond the range of composition space spanned by the experimental data set. Our enstatite composition of 0.07 wt. % Fe for the aubrite meteorites is outside the range covered by their analysis. Nonetheless, the results of Wade and Wood at face value suggest FeO activity coefficients near unity. For completeness, we also perform our calculations with $\gamma^{silicate}_{FeO} = 1$ to explore the sensitivity of the results to this activity coefficient. The resulting values for A are $2.33 \times 10^5 \pm 5.3 \times 10^4$ for Norton County and $2.14 \times 10^5 \pm 2.8 \times 10^4$ for Mount Egerton. The relationship between temperature, oxygen fugacity, and FeO activity coefficient as calculated using Eq. (2) is plotted in Fig. 9. The figure shows explicitly that a lower gamma value yields a higher temperature of equilibration. A higher temperature of equilibration yields a closer agreement between the Fe fractionation factor between metal and silicate between in our study and that from the experimental work of Elardo and Shahar (2017).

Because the exact value of the activity coefficient for FeO in silicate is not known, and because the oxygen fugacity calculated for a given temperature and Si concentration in metal depends on this coefficient, we derive a range of temperatures from Eq. (2) by applying a range of values for both f_{O_2} and $\gamma^{silicate}_{FeO}$ (shaded region in Fig. 9). Fig. 10 shows several representative fractionation vs. temperature

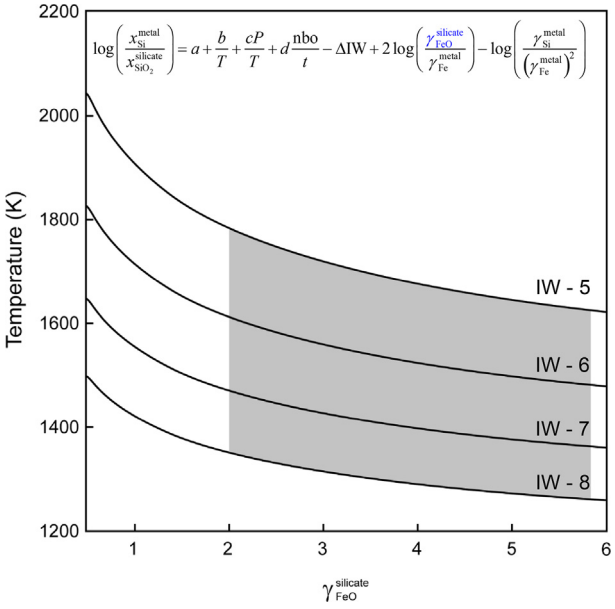

Fig. 9. Equilibration temperatures for the aubrite meteorite Norton County as a function of oxygen fugacity (curves) and the activity coefficient of FeO in the silicate melt (abscissa). The shaded region shows the plausible regime of temperatures based on the likely values of the parameters in question (see text). We consider a value of ~IW – 6.5 for the aubrite meteorites based on the literature data. Ranges in the FeO activity coefficients are discussed in the text.

curves that are dependent on f_{O_2} and $\gamma_{FeO}^{silicate}$. For what follows we adopt the temperatures of 1415 K for Norton County and 1460 K for Mount Egerton, as these values take into consideration the high MgO value of the rocks and are consistent with the relevant melting experiments.

4.3. Implications for metal core formation

With an estimate for the equilibration temperature, and thus the temperature-dependent equilibrium metal-silicate Fe isotope fractionation, we examine what this information reveals about the cores of planetesimals. We use Vesta as an example of planetesimal core formation. Thermal models of Vesta show that the core reached a temperature of ~1800 K (Zhou et al., 2013). We use our Fe metal-silicate fractionation calibrations for temperatures of 1415 K and 1460 K for the Norton County and Mount Egerton meteorites, respectively, in conjunction with mass balance, to calculate the δ^{57}Fe values for the silicate and metallic phases of a body as a function of core size for a Vesta-sized body based on an iron equilibration temperature of ~1800 K. The mass balance equation is

$$\delta^{57}Fe_{metal} = \delta^{57}Fe_{bulk} + x_{Fe}^{silicate}\Delta^{57}Fe_{metal-silicate}(T) \quad (4)$$

where here $x_{Fe}^{silicate}$ refers to the fraction of total iron present as silicate (not to be confused with the concentration of Fe in silicate). We use our measured $\Delta^{57}Fe_{metal\text{-}silicate}$ and Eq. (4) to determine the fractions of Fe in silicates and metals

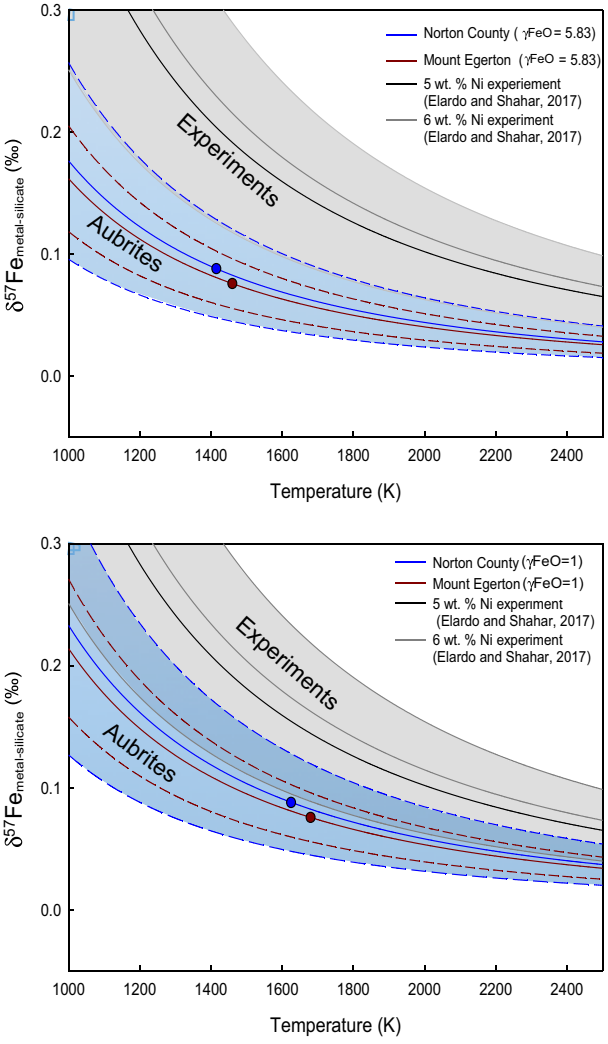

Fig. 10. Comparison of Fe metal-silicate fractionation in natural samples (this study) and experiments (Elardo and Shahar, 2017). The curves are temperature calibrations derived from the measured fractionations. Upper panel: aubrite fractionation curves based on $\gamma_{FeO}^{silicate} = 5.83$. Lower panel: aubrite fractionation curves based on $\gamma_{FeO}^{silicate} = 1.0$. The dashed lines represent the uncertainties in temperature from uncertainties in $\gamma_{FeO}^{silicate}$ and the uncertainties in our measurements. The blue field encompasses the full range in aubrite fractionation factors including uncertainties. For the experimental data from Elardo and Shahar (2017) we show Ni contents of 5 and 6 wt.%, falling within the range for the aubrites in this study. Uncertainties for the experimental data are encompassed by the grey regions in both plots and reflect the uncertainties in the measured $\Delta^{57}Fe_{metal\text{-}silicate}$ values. (For interpretation of the references to colour in this figure legend, the reader is referred to the web version of this article.)

that allow for the iron cores to have higher $^{57}Fe/^{54}Fe$ than the silicate mantles.

The $\Delta^{57}Fe_{metal\text{-}silicate}$ that we derive from the aubrites is specific to ~5.4 wt.% Ni on average. When considering a Vesta-sized body with a core, we look to the magmatic iron meteorites as a proxy for Vesta's core chemistry to obtain a

more realistic concentration of non-iron constituents in the metal. Although the values for Ni contents of iron meteorites ranges from 5 to 60 wt.%, the vast majority fall between 5 and 12 wt.%, with an average of ~8–10 wt.% for magmatic iron meteorites (Goldstein et al., 2009). Estimates for the Ni concentrations in the core of Vesta are also highly variable (e.g., Righter and Drake, 1997; Dreibus and Wänke, 1980).

Confounding the uncertainties in core composition is the fact that the core S concentrations are important but highly uncertain. Magmatic iron meteorites are the solid metal that formed by fractional crystallization from the parental metallic melt. Troilite nodules in these meteorites crystallized from trapped metallic liquid and the nodules are evidence for the presence of S in the parent body core. The solubility of S in the solid metal is low, which inhibits determination of the S concentration of the parental melt through direct measurements of iron meteorites as there is no S in the crystallized metal (Chabot, 2004). Estimates of the S content of the parental melt range from less than 1 wt.% up to 17 wt.% S (Willis and Goldstein, 1982; Jones and Drake, 1983; Haak and Scott, 1993; Ulff-Møller, 1998; Wasson, 1999; Wasson and Richardson, 2001; Wasson and Choi, 2003; Chabot, 2004). Between the Ni and possible S contents, there is potentially a rather large non-iron component in the parental melt (up to ~27 wt.%), which may significantly affect Fe isotope metal-silicate fractionation.

In order to accommodate the more typical Ni and S contents we use the variation in fractionation with composition, $d\Delta^{57}\mathrm{Fe}/dx_{\mathrm{sub}}$, where x_{sub} is the atom per cent of Ni + S in the metal, from Elardo and Shahar combined with our average measured metal/silicate fractionation factor from the aubrites to arrive at the expression

$$\Delta^{57}Fe_{metal-silicate} = \left\{1.75 \times 10^5 + 5.048 \times 10^4 (x_{sub} - 5.1)\right\}/T^2. \quad (5)$$

For this equation we use the average A value for the temperatures of equilibration obtained using $\gamma\mathrm{FeO} = 5.83$. The value 5.1 in Eq. (5) is the average x_{sub} for the two aubrites (Ni = 5.1 atom%). The results from Eq. (5) are not critically sensitive to the choice of γFeO, with shifts of ~0.005‰ when changing γFeO from 1 to 5.8 at 1800 K (Figs. 9 and 10). In what follows we hold the Ni concentration at 9 at.% in Eq. (5) and leave the S concentration as a variable that controls the magnitude of $\Delta^{57}\mathrm{Fe}_{\text{metal-silicate}}$ since the original sulfur concentration in the metal melt is poorly constrained. However, we emphasize that according to the Elardo and Shahar formulation, substitution of Ni and S have the same effect on the metal-silicate Fe isotope fractionation factor; the controlling factor in Eq. (5) is not the Ni concentration alone, nor the S concentration alone, but rather the sum of the two.

The assumption that $\delta^{57}\mathrm{Fe}_{\mathrm{bulk}}$ for iron meteorite parent bodies is chondritic is often made, but there are reasons to question this assumption. Hin et al. (2017) found that chondrites are ~0.02 to ~0.04‰ lower in $^{25}\mathrm{Mg}/^{24}\mathrm{Mg}$ than Earth, Mars, eucrites, and angrites. There is a similar disparity in Si isotope ratios between chondrites and differentiated bodies (Georg et al., 2006; Ziegler et al., 2010; Savage and Moynier, 2013; Zombardi et al., 2013; Pringle et al., 2014). The modeling by Hin et al. suggests that this heavy isotope signature of various planetary bodies can result from evaporation of molten rock after collisions during the accretionary growth phase of planetesimals. This effect would have similar, somewhat larger consequences for Fe if iron metal was involved in the evaporation process (Young, 2000). As a result, iron meteorite parent bodies may have accreted from objects that were already high in $^{57}\mathrm{Fe}/^{54}\mathrm{Fe}$ relative to chondrite. For this reason, we leave the bulk iron isotope composition as a free parameter when modeling the isotopic constraints on the relative masses of core and mantle in the discussion that follows.

Fig. 11 shows the calculated core mass fractions of planetesimals as a function of the bulk $^{57}\mathrm{Fe}/^{54}\mathrm{Fe}$ composition of the bodies based on Eqs. (4) and (5). We convert $X^{\mathrm{Fe}}_{\mathrm{silicate}}$, the fraction of total iron present in silicate, to core mass fraction by fixing the mole fraction of FeO in silicate to 0.05. This mole fraction yields $\Delta\mathrm{IW} = -2.5 \pm 0.2$ when paired with the metal compositions implied by the fractionation factor (based on $\Delta\mathrm{IW} = 2\ \log\ (x\mathrm{FeO}_{\mathrm{silicate}}/x\mathrm{Fe}_{\mathrm{metal}})$ where $x\mathrm{FeO}_{\mathrm{silicate}}$ is the mole fraction of the FeO component in silicate, $x\mathrm{Fe}_{\mathrm{metal}}$ is the mole fraction of Fe comprising the metal, and activity coefficients are taken as unity). This oxygen fugacity is consistent with estimates for Vesta (Steenstra et al., 2016). The four curves shown in the figure correspond to fixed $\delta^{57}\mathrm{Fe}$ values for cores and mantles that span the relevant ranges and combinations of these values. The $\delta^{57}\mathrm{Fe}$ values of the core and mantle for each curve can

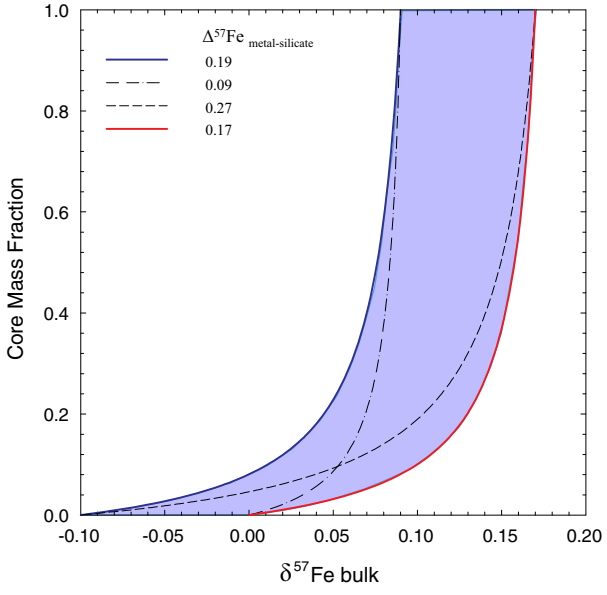

Fig. 11. Core fractions and bulk Fe isotopic compositions of planetesimals determined using Eqs. (4) and (5). Solutions that yield $\delta^{57}\mathrm{Fe}$ of cores similar to those of iron meteorites, $\delta^{57}\mathrm{Fe}$ values of silicates consistent with HED meteorites, and estimates of the vestian mantle (see text) are within the shaded region. The core and silicate $\delta^{57}\mathrm{Fe}$ values represented by each curve can be read where the curves intersect core fractions of 1 and 0, respectively.

be read from the curves at core mass fractions of 1 and 0, respectively. The curves are calculated by choosing $\Delta^{57}Fe_{metal\text{-}silicate}$ and $\delta^{57}Fe_{bulk}$ such that iron cores and silicate mantles have $\delta^{57}Fe$ values of 0.09 to 0.17‰ (i.e., $\delta^{57}Fe$ metal $= 0.13 \pm 0.04$‰) and 0.00 to −0.10‰, respectively. The range in metal values is suggested by that exhibited by iron meteorites. The high end of the range for silicate values is constrained by values for silicates in HED meteorites that average near zero (Fig. 1). The lower end of the silicate range is based on the suggestion by Elardo and Shahar (2017) that planetesimal silicates were subchondritic, and in particular that the vestan mantle is ~−0.10‰. If this is correct, the HED basalts are chondritic by happenstance. By fixing atomic% Ni at 9 when calculating $\Delta^{57}Fe_{metal\text{-}silicate}$, the typical Ni concentration for iron meteorites, variations in the metal-silicate fractionation factor at fixed temperature correspond to variations in atom% S (Eq. (5)).

The left bound of the shaded region in Fig. 11 corresponds to a $\Delta^{57}Fe_{metal\text{-}silicate}$ of 0.19‰, and a Ni + S concentrations in the metal of 13.8 atom%. The core and mantle $\delta^{57}Fe$ values for this curve are 0.09 and −0.10‰, respectively, and so this curve derives from the lowest relevant $\delta^{57}Fe$ values for both core and mantle. The right bound of the shaded area in Fig. 11 corresponds to $\Delta^{57}Fe_{metal\text{-}silicate} = 0.17$‰ and a Ni + Si concentration of 12.5 atom%. The $\delta^{57}Fe$ values for core and mantle for this curve are 0.17‰ and 0.00‰, respectively, and so give the solution where the values are highest for both core and mantle. The two additional curves in Fig. 11 represent the smallest and largest $\Delta^{57}Fe_{metal\text{-}silicate}$ values that can satisfy simultaneously the ranges in $\delta^{57}Fe$ values of iron meteorites and coexisting silicates as described above. The lowest $\Delta^{57}Fe_{metal\text{-}silicate}$ value of 0.09‰ corresponds to a Ni + S concentration of 7.4% while the highest $\Delta^{57}Fe_{metal\text{-}silicate}$ value of 0.27‰ corresponds to a Ni + S concentration of 18.9%.

The curves in Fig. 11 show that the common assumption that $\delta^{57}Fe_{bulk}$ is chondritic requires small core fractions of ≤8% by mass. The observed elevated $^{57}Fe/^{54}Fe$ ratios among magmatic iron meteorites relative to chondrites is difficult to explain using the fractionation between silicate and metal that we observe in the meteorites themselves unless the core fractions of the parent bodies were small. Based on what we know about rocky bodies in our solar system, core fractions of <8% seem unlikely, suggesting instead that planetesimals from which the iron meteorites derive had relatively high bulk $^{57}Fe/^{54}Fe$ values compared to chondrites as the result of evaporation.

For Vesta-like bodies with core mass fractions of 0.18 (Russell et al., 2012; Szurgot, 2015), the results in Fig. 11 suggest $\delta^{57}Fe_{bulk}$ values of 0.04‰ to 0.13‰. Bodies with Earth-like core fractions of 0.33 by mass require $\delta^{57}Fe_{bulk}$ values of 0.06 to 0.15‰, depending on the metal Ni + S concentrations. Models of Fe isotope fractionation due to evaporation of melts exposed to the surfaces of planetesimals will be required to determine which of the two factors, evaporation or small core fractions, is the more plausible explanation for high $\delta^{57}Fe$ values among iron meteorites.

Zinc and Cu are moderately volatile elements that might be expected to exhibit the effects of elemental evaporation given the evidence for evaporation of the more refractory Mg, Si, and Fe. While the average $^{66}Zn/^{64}Zn$ of magmatic iron meteorites is 0.4‰ greater than that for unaltered carbonaceous chondrites and terrestrial rocks based on the data from Chen et al. (2013) and Luck et al. (2005), the variability among these irons is ±0.6‰ 1σ (Chen et al., 2013), rendering the distinction marginal. The $^{65}Cu/^{63}Cu$ isotope ratios of iron meteorites are not clearly distinct from chondrites and terrestrial rocks in general (Bishop et al., 2012; Chen et al., 2016). For both Zn and Cu there is a notable absence of correlations between isotope ratios and concentrations, contrary to expectations for these minor elements if they were subjected to a simple history of volatilization. We infer that isotopic signatures of volatilization may be more faithfully recorded in major elements like Mg, Si, and Fe than in the minor and trace moderately volatile elements. Nickel has a similar volatility to that of Fe and is another element that might record the effects of volatilization. To date, the Ni isotope ratio data are inconclusive with respect to fractionations between chondrites and differentiated bodies at the ≤0.05‰ per amu level that is subject of this study (Cook et al., 2007; Moynier et al., 2007), perhaps in part due to sub-solidus diffusion effects on Ni isotope ratios in metals (Chernonozhkin et al., 2016).

Finally, we consider the possibility for sub-solidus equilibration at the temperatures previously obtained for the aubrites. In this case, the sub-solidus temperatures 1130 K for Norton County and 1200 K for Mount Egerton are assumed to be correct (Wasson et al., 1994). If the lower temperatures of equilibration are in fact correct for iron isotope exchange, as depicted in Fig. 4, it becomes impossible to attribute the differences in Fe isotope compositions of iron meteorites and silicates in the early solar system, as represented by vestan silicates and chondrites, to simple core formation. Post-formation evaporation would then be necessitated by the data. Consistency between theory, experiments, and measurements for metal-silicate Si isotope partitioning in these rocks as described by Ziegler et al. (2010) argues for the lower temperatures of equilibration for Si. If the equilibration temperatures for Si isotopes between silicate and metal for these rocks are taken to be the higher temperatures derived in this study for Fe, then the measured aubrite silicate-metal Si isotope fractionation factors would be greater than estimates from theory and experiments by ~1‰ (Ziegler et al., 2010).

These observations raise the possibility that Si isotope exchange between metal and silicate in these rocks persisted to lower (sub-solidus) temperatures than Fe isotope exchange. There is evidence for this in relevant diffusion coefficients. As an illustration, we compare Si and Fe isotope closure temperatures, T_C, using the Dodson formulation for T_C as a function of the radius of the mineral phases of interest, rate of cooling, and diffusivity (Dodson, 1973). Even just the outermost margins of enstatite grains have sufficient Si to act as effectively infinite sources of Si for exchange with the comparatively low mass of Si in the adjacent metal grains. As a result, even slow diffusion of Si in enstatite is sufficient to permit isotope exchange with Si in the metal phase. Diffusion of Si in metal

is thus the limiting factor for T_C in the case of Si isotope exchange. We use the temperature-dependent self-diffusion coefficient of Si in Fe silicide given by Riihimaki et al. (2008) to calculate T_C. Setting the radius of the metal to 2.6 mm and the rate of cooling to 0.1 deg yr^{-1} (these values are by way of example and are not a unique solution) one obtains a T_C for Si isotope exchange of 1130 K that matches the low temperature for Norton County that is consistent with the observed metal-silicate Si isotopic fractionation (Ziegler et al., 2010). Iron isotope exchange may have been limited by Fe diffusion in the silicate phase because metal is essentially an infinite reservoir of Fe for exchange with the Fe-poor enstatite. The cations Fe^{2+} and Mg^{2+} occupy the same crystallographic sites in enstatite, suggesting that Fe isotopes migrate by temperature-dependent Fe-Mg interdiffusion. We use the Fe-Mg diffusion coefficient for enstatite of Dohmen et al. (2016) to estimate T_C for iron isotope exchange between metal and enstatite. With the same crystal size and cooling rate as used for Si, the iron isotope T_C is 1480 K. We take this higher, super-solidus closure temperature for Fe compared to the sub-solidus T_C for Si to mean that Si isotope exchange may have persisted to sub-solidus temperatures (1130 K) whereas Fe isotope exchange ceased as the rock solidified at $T < \sim 1470$ K.

5. CONCLUSIONS

We determined the Fe isotope fractionation between the metal and silicate phases of two aubrite meteorites, Norton County and Mount Egerton. We find that the metallic phase is high in $^{57}Fe/^{54}Fe$ with respect to the silicate phase, and that $\Delta^{57}Fe_{metal\text{-}silicate}$ is 0.08‰ for Mount Egerton and 0.09‰ for Norton County. Based on prior work suggesting isotope partitioning at equilibrium, two different cases were explored for estimating the temperature of equilibration. In the lower temperature case, we use the temperatures of equilibration calculated with the method of Wasson et al. (1994), 1130 K for Norton County and 1200 K for Mount Egerton. In this case, we are unable to explain the observed difference in the Fe isotope compositions of magmatic iron meteorites and chondrites as being the result of planetesimal differentiation.

In the higher temperature scenario, we use updated activity models and adopt a range of activity coefficients for FeO in the silicate melt with corresponding ranges in oxygen fugacity. The updated activity models suggest higher temperatures of equilibration of 1415 K for Norton County and 1460 K for Mount Egerton. If these temperatures are correct, we are able to explain the iron and chondrite meteorite data through differentiation under very restrictive conditions. If the parent bodies of the iron meteorites had chondritic bulk $^{57}Fe/^{54}Fe$, their cores must have been unusually small (~8% by mass or less). Relaxing the constraint that the bodies were chondritic in their bulk iron isotope ratios allows for larger core mass fractions commensurate with usual expectations for planetesimals. In this case, the elevated $^{57}Fe/^{54}Fe$ values of iron meteorites are due in part to evaporation of melt during the accretion stages of the parent bodies and not solely the result of metal-silicate differentiation.

ACKNOWLEDGEMENTS

We would like to thank Edwin Schauble and Anat Shahar for helpful discussions, Carl Agee for providing us with the Norton County sample, and John Wasson for providing us with the Mount Egerton sample, the iron meteorite samples, and useful discussions. Funding was provided by NASA grant NNX15AH43G to EDY.

REFERENCES

Baker J. A., Schiller M. and Bizzaro M. (2012) ^{26}Al-^{29}Mg deficit dating ultramafic meteorites and silicate planetesimals differentiation in the early Solar System. *Geochim. Cosmochim. Acta* **77**, 415–431.

Berthet S., Malavergne V. and Righter K. (2009) Melting of the Indarch Meteorite (EH4 Chondrite) at 1 GPa and variable oxygen fugacity: implications for early planetary differentiation processes. *Geochim. Cosmochim. Acta* **73**, 6402–6420.

Bishop M. C., Moynier F., Weinstein C., Fraboulet J.-G., Wang K. and Foriel J. (2012) The Cu isotopic composition of iron meteorites. *Meteorit. Planet. Sci.* **47**, 268–276.

Casanova I., Keil K. and Newsom H. E. (1993) Composition of metal in aubrites: constraints on core formation. *Geochim. Cosmochim. Acta* **57**, 675–682.

Chabot N. L. (2004) Sulfur contents of the parental metallic cores of magmatic iron meteorites. *Geochim. Cosmochim. Acta* **68**, 3607–3618.

Chabot N. L. and Jones J. H. (2003) The parameterization of solid-liquid metal partitioning of siderophile elements. *Meteorit. Planet. Sci.* **38**, 1425–1436.

Chen H., Nguyen B. N. and Moynier F. (2013) Zinc isotopic composition of iron meteorites: absence of isotopic anomalies and origin of the volatile element depletion. *Meteorit. Planet. Sci.* **48**, 2441–2450.

Chen H., Moynier F., Humayun M., Bishop A. and Williams J. T. (2016) Cosmogenic effects on Cu isotopes in IVB iron meteorites. *Geochim. Cosmochim. Acta* **182**, 145–154.

Chernonozhkin S. M., Goderis S., Costas-Rodriguez M., Claeys P. and Vanhaecke F. (2016) Effect of parent body evolution on equilibrium and kinetic isotope fractionation: a combined Ni and Fe isotope study of iron and stony-iron meteorites. *Geochim. Cosmochim. Acta* **186**, 168–188.

Clayton R. N. and Mayeda T. K. (1996) Oxygen isotope studies of achondrites. *Geochim. Cosmochim. Acta* **60**, 1999–2017.

Clayton R. N., Mayeda T. K. and Rubin A. E. (1984) Oxygen isotopic compositions of enstatite chondrites and aubrites. *J. Geophys. Res.* **89**, C245–C249.

Cook D. L., Wadhwa M., Clayton R. N., Nl Daupha, Janney P. E. and Davis A. M. (2007) Mass-dependent fractionation of nickel isotopes in meteoritic metal. *Meteoritic. Planet. Sci.* **12**, 2067–2077.

Corgne A., Keshav S., Wood B. J., McDonough W. F. and Fei Y. (2008) Metal-silicate partitioning and constraints on core composition and oxygen fugacity during Earth accretion. *Geochim. Cosmochim. Acta* **72**, 574–589.

Craddock P. R. and Dauphas N. (2011) Iron isotope compositions of geological reference materials and chondrites. *Geostand. Geoanal. Res.* **35**, 101–123.

Dauphas N., Craddock P. R., Asimow P. D., Bennett V. C., Nutman A. P. and Ohnenstetter D. (2009a) Iron isotopes may

reveal the redox conditions of mantle melting from Archean to present. *Earth Planet. Sci. Lett.* **288**, 255–267.

Dauphas N., Pourmand A. and Teng F.-Z. (2009b) Routine isotopic analysis of iron by HR-MC-ICPMS: how precise and how accurate? *Chem. Geol.* **267**, 175–184.

Dodson M. H. (1973) Closure temperature in cooling geochronological and petrological problems. *Contrib. Mineral. Petrol.* **40**, 259–274.

Dohmen R., Ter Heege J. H., Becker H. W. and Chakraborty S. (2016) Fe-Mg interdiffusion in orthopyroxene. *Am. Mineral.* **101**, 2210–2221.

Dreibus G. and Wänke H. (1980) The bulk composition of the eucrite parent asteroid and its bearing on planetary evolution. *Z. Naturforsch.* **35a**, 204–206.

Elardo S. M. and Shahar A. (2017) Non-chondritic iron isotope ratios in planetary mantles as a result of core formation. *Nat. Geosci.* **10**, 317–321.

Georg R. B., Halliday A. N., Schauble E. A. and Reynolds B. C. (2006) Silicon in the Earth's core. *Nature* **447**, 1102–1106.

Goldstein J. I., Scott E. R. D. and Chabot N. L. (2009) Iron meteorite: crystallization, thermal history, parent bodies and origin. *Chem. Erde-Geochem.* **69**, 293–325.

Haak H. and Scott E. R. D. (1993) Chemical fractionations in group IIIAB iron meteorites: origin by dendritic crystallization of an asteroidal core. *Geochim. Cosmochim. Acta* **57**, 3457–3472.

Hin R. C., Schmidt M. W. and Bourdon B. (2012) Experimental evidence for the absence of iron isotope fractionation between metal and silicate liquids at 1 GPa and 1250–1300 °C and its cosmochemical consquences. *Geochem. Cosmochem. Acta* **77**, 164–181.

Hin R. C., Coath C., Carter P. J., Nimmo F., Lai Y.-J., Pogge von Strandmann P. A. E., Willbold M., Leinhardt Z., Walter M. and Elliott T. (2017) Magnesium isotope evidence that accretional vapour loss shapes planetary compositions. *Nature* **549**, 511–515.

Hopp T., Fischer-Gödde M. and Klein T. (2018) Ruthenium isotope fractionation in protoplanetary cores. *Geochim. Cosmochim. Acta* **223**, 75–89.

Horn I., von Blanckenburg F., Schoenberg R., Steinhoefel G. and Markl G. (2006) In situ iron isotope ratio determination using UV-femtosecond laser ablation with application to hydrothermal ore formation processes. *Geochim. Cosmochim. Acta* **70**, 3677–3688.

Holzheid A., Palme H. and Chakraborty S. (1997) The activities of NiO, CoO, and FeO in silicate metls. *Chem. Geol.* **139**, 21–38.

Jones J. H. and Drake M. J. (1983) Experimental investigations of trace element fractionation in iron meteorites, II: the influence of sulfur. *Geochim. Cosmochim. Acta* **47**, 1199–1209.

Kehm K., Hauri E. H., Alexander C. M. O'D. and Carlson R. W. (2003) High precision iron isotope measurements of meteoritic material by cold plasma ICP-MS. *Geochim. Cosmochim. Acta* **67**, 2879–2891.

Keil K. (2010) Enstatite achondrite meteorites (aubrites) and the histories of their asteroidal parent bodies. *Chem. Erde-Geochem.* **70**, 295–317.

Laramir J. W. (1968) Experimental studies on the system Fe-MgO-SiO_2-O_2 and their bearing on the petrology of chondritic meteorites. *Geochim. Cosmochim. Acta* **32**, 1187–1207.

Luck J.-M., Othman D. B. and Albarede F. (2005) Zn and Cu isotopic variations in chondrites and iron meteorites: early solar nebula reservoirs and parent-body processes. *Geochim. Cosmochim. Acta* **69**, 5351–5363.

McCall G. J. H. (1965) A meteorite of unique type from Western Australia: the Mount Egerton stony-iron. *Miner. Mag.* **35**, 241–249.

McCoy T. J., Dickinson T. L. and Lofgren G. E. (1999) Partial melting of the Indarch (EH4) meteorite: a textural, chemical, and phase relations view of melting and melt migration. *Meteorit. Planet. Sci.* **34**, 735–746.

Moynier F., Blichert-Toft J., Telouk P., Luck J.-M. and Albarede F. (2007) Comparative stable isotope geochemistry of Ni, Cu, Zn, and Fe in chondrites and iron meteorites. *Geochim. Cosmochim. Acta* **71**, 4365–4379.

Okada A., Keil K., Taylor J. and Newsom H. (1988) Igneous history of the aubrite parent asteroid—evidence from the Norton County enstatite achondrite. *Meteoritics* **23**, 59–74.

Poitrasson F., Halliday A. N., Lee D., Levasseur S. and Teutsch N. (2004) Iron isotope differences between Earth, Moon, Mars and Vesta as possible records of contrasted accretion mechanism. *Earth Planet. Sci. Lett.* **223**, 253–266.

Poitrasson F., Levasseur S. and Teutsch N. (2005) Significance of iron isotope mineral fractionation in pallasites and iron meteorites for the core-mantle differentiation of planets. *Earth Planet. Sci. Lett.* **234**, 151–164.

Poitrasson F., Roskosz M. and Corgne A. (2009) No iron isotope fractionation between molten alloys and silicate melt to 2000 ° C and 7.7 GPa: Experimental evidence and implications for planetary differentiation and accretion. *Earth Planet. Sci. Lett.* **278**, 376–385.

Polyakov V. B., Clayton R. N., Horita J. and Mineev S. D. (2007) Equilibrium iron isotope fractionation factors of minerals: reevaluation from the data of nuclear inelastic resonant X-ray scattering and Mössbauer spectroscopy. *Geochim. Cosmochim. Acta* **71**, 3833–3846.

Pringle E. A., Moynier F., Savage P. S., Badro J. and Barrat J.-A. (2014) Silicon isotopes in angrites and volatile loss in planetesimals. *Proc. Natl. Acad. Sci.* **111**, 17029–17032.

Righter K. and Drake M. J. (1997) Magma ocean on Vesta: core formation and petrogenesis of eucrites and diogenites. *Meteorit. Planet. Sci.* **32**, 929–944.

Righter, K., Drake, M.J., Scott, E., 2006. Compositional Relationships Between Meteorites and Terrestrial Planets. In: Lauretta, D.S., McSween, Jr. H.Y. (Eds.), Meteorites and the Early Solar System II. University of Arizona Press, Tucson, in collaboration with Lunar and Planet. Inst., Houston, pp. 803–828.

Riihimaki I., Virtanen A., Pusa P., Salamon M., Mehrer H. and Raisanen J. (2008) Si self-diffusion in cubic B20-structure FeSi. *Europhys. Lett.* **82**, 3 pp.

Roskosz M., Luais B., Watson H. C., Toplis M. J., Alexander C. M. O'D. and Mysen B. O. (2006) Experimental quantification of the fractionation of Fe isotopes during metal segregation from a silicate melt. *Earth Planet. Sci. Lett.* **248**, 851–867.

Russell C. T., Raymong C. A., Coradini A., McSween H. Y., Zuber M. T., Nathues A., De Sanctis M. C., Jaumann R., Konopliv A. S., Asmar Preusker F., Park S. W., Gaskell R., Keller H. U., Mottola S., Roatsch T., Scully J. E. C., Smith D. E., Tricarico P., Toplis M. J., Christensen U. R., Feldman W. C., Lawrence D. J., McCoy T. J., Prettyman T. H., Reedy R. C., Sykes M. E. and Titus T. N. (2012) Dawn at Vesta: testing the protoplanetary paradigm R. S. *Science* **336**, 684–688.

Savage P. S. and Moynier F. (2013) Silicon isotopic variation in enstatite meteorites: clues to their origin and Earth-forming material. *Earth Planet. Sci. Lett.* **361**, 487–496.

Schoenberg R. and von Blanckenburg F. (2006) Modes of planetary-scale Fe isotope fractionation. *Earth Planet. Sci. Lett.* **252**, 342–359.

Scott E. R. D. (1972) Chemical fractionation in iron meteorites and its interpretation. *Geochim. Cosmochim. Acta* **36**, 1205–1236.

Scott E. R. D. and Wasson J. T. (1975) Classification and properties of iron meteorites. *Rev. Geophys. Space Phys.* **13**, 527–546.

Shahar A., Hillgren V. J., Horan M. F., Mesa-Garcia J., Kaufman L. A. and Mock T. D. (2015) Sulfur-controlled iron isotope fractionation experiments of core formation in planetary bodies. *Geochim. Cosmochim. Acta* **150**, 253–264.

Shahar A., Ziegler K., Young E. D., Ricolleau A., Schauble E. A. and Fei Y. W. (2009) Experimentally determined Si isotope fractionation between silicate and Fe metal and implications for Earth's core formation. *Earth Planet. Sci. Lett.* **288**, 228–234.

Steenstra E. S., Knibb J. S., Rai N. and van Westrenen W. (2016) Constraints on core-formation in Vesta from metal-silicate partitioning of siderophile elements. *Geochim. Cosmochim. Acta* **177**, 48–61.

Szurgot M. (2015) Core mass fraction and mean atomic weight of terrestrial planets, Moon, and protoplanet Vesta. *Compar. Tect. and Geodynam. Conf.*, 5001.

Ulff-Møller F. (1998) Effects of liquid immiscibility on trace element fractionation in magmatic iron meteorites: a case study of group IIIAB. *Meteorit. Planet. Sci.* **33**, 207–220.

Wade J. and Wood B. J. (2005) Core formation and the oxidation state of the Earth. *Earth Planet. Sci. Lett.* **236**, 78–95.

Wait C. M. (1970) The metal phase of Horse Creek, Mount Egerton, and Norton County enstatitic meteorites. *Mineral. Mag.* **37**, 905–908.

Wang K., Moynier F., Dauphas N., Barrat J.-A., Craddock P. and Sio C. K. (2012) Iron isotope fractionation in planetary crusts. *Geochim. Cosmochim. Acta* **89**, 31–45.

Wang K., Savage P. S. and Moynier F. (2014) The iron isotope composition of enstatite meteorites: implications for their origin and the metal/sulfide Fe isotopic fractionation factor. *Geochim. Cosmochim. Acta* **142**, 149–165.

Wasson J. T. (1999) Trapped melt in IIIAB irons; solid/liquid elemental partitioning during the fractionation of the IIIAB magma. *Geochim. Cosmochim. Acta* **63**, 2875–2889.

Wasson J. T. and Choi B.-G. (2003) Main-group pallasites: chemical composition, relationship to IIIAB irons, and origin. *Geochim. Cosmochim. Acta* **67**, 3079–3096.

Wasson J. T., Kallemeyn G. W. and Rubin A. E. (1994) Equilibration temperatures of EL chondrites: a major downward revision in the ferrosilite contents of enstatite. *Meteoritics* **29**, 658–662.

Wasson J. T. and Richardson J. W. (2001) Fractionation trends among IVA iron meteorites: contrasts with IIIAB trends. *Geochim. Cosmochim. Acta* **65**, 951–970.

Wasson J. T. and Wai C. M. (1970) Composition of metal, schreibersite, and perryite of enstatite achondrites and the origin of enstatite chondrites and achondrites. *Geochim. Cosmochim. Acta* **34**, 169–184.

Watters T. R. and Prinz M. (1979) Aubrites: their origin and relationship to enstatite chondrites. *Lunar Planet. Sci. Conf. X*, 1073–1093.

Watters T. R. and Prinz M. (1980) Mt. Egerton and the aubrite parent body. *L Lunar Planet. Sci. Conf.* **XI**, 1225–1227.

Watters T. R., Prinz M., Rambaldi E. R. and Wasson J. T. (1980) ALHA 78113, Mt. Egerton and the aubrite parent body. *Meteoritics* **15**, 386.

Weyer S., Anbar A. D., Brey G. P., Muncker C. and Woodland A. B. (2005) Iron isotope fractionation during planetary differentiation. *Earth Planet. Sci. Lett.* **240**, 251–265.

Weyer S. and Ionev D. A. (2007) Partial melting and melt percolation in the mantle: the message from Fe isotopes. *Earth Planet. Sci. Lett.* **259**, 119–133.

Williams H. M., Markowski A., Quitté G., Halliday A. N., Teutsch N. and Levasseur S. (2006) Fe isotope fractionation in iron meteorites: new insights into metal-sulphide segregation and planetary accretion. *Earth Planet. Sci. Lett.* **250**, 486–500.

Willis J. and Goldstein J. I. (1982) The effects of C, P, and S on trace element partitioning during solidification in Fe-Ni alloys. *J. Geophys. Res.* **87**, A435–A445.

Wood B. J. and Wade J. (2013) Activities and volatilities of trace components in silicate melts: a novel use of metal-silicate partitioning data. *Miner. Petrol.* **166**, 911–921.

Young E. D. (2000) Assessing the implications of K isotope cosmochemistry for evaporation in the preplanetary solar nebula. *Earth Planet. Sci. Lett.* **183**, 321–333.

Zhou Q., Yin Q.-Z., Young E. D., Li X.-H., Wu F.-Y., Li Q.-L., Liu Y. and Tang G.-Q. (2013) SIMS Pb-Pb and UPb age determination of eucrite zircons at <5 μm scale and the first 50 Ma of thermal history of Vesta. *Geochem. Cosmochim. Acta* **110**, 152–175.

Zhu X. K., Guo Y., Williams R. J. P., O'Nions R. K., Matthews A., Belshaw N. S., Canters G. W., de Waal E. C., Weser U., Burgess B. K. and Salvato B. (2002) Mass fractionation processes of transition metal isotopes. *Earth Planet Sci., Lett.* **200**, 47–62.

Ziegler K., Young E. D., Schauble E. A. and Wasson J. T. (2010) Metal-silicate silicon isotope fractionation in enstatite meteorites and constraints on Earth's core formation. *Earth Planet. Sci. Lett.* **295**, 487–496.

Zombardi T., Poitrasson F., Corgne A., Meheut M., Quitte G. and Anand M. (2013) Silicon isotope variations in the inner solar system: implications for planetary formation, differentiation and composition. *Geochem. Cosmochim. Acta* **121**, 67–83.

Associate editor: Frederic Moynier